

Trends in observed surface solar radiation and their causes in Brazil in the first two decades of the 21st century.

Lucas Ferreira-Correa¹, Doris-Folini¹, Boriana-Chtirkova¹, and Martin Wild¹

¹Institute for Atmospheric and Climate Sciences, ETH Zurich, Zurich, Switzerland.

Correspondence to: Lucas Ferreira Correa (lucas.ferreira@env.ethz.ch)

Abstract. Numerous studies have investigated the long term variability of surface solar radiation (SSR) around the world. However, the large disparity in the availability of observational data between developed and least developed/developing countries leads to an underrepresentation of studies on SSR changes in the latter. This is especially true for South America, where few observational studies have investigated the SSR trends, and usually only at a local or regional scale. In this study we use data from 34 stations distributed throughout all the regions of Brazil to present the SSR trends in the first two decades of the 21st century and investigate their associated causes. The stations were grouped into 8 composites according to their proximity. Our results show that in the North and Northeast Brazil a strong dimming occurred, with significant contributions from increasing atmospheric absorption, most likely due to anthropogenic emissions, and increasing cloud cover. In the Southeast and Midwest regions of Brazil near-zero trends resulted from competing effects of clear-sky processes (attenuation of solar radiation under cloudless conditions) and strong negative trends in cloud cover. In the South part of the Amazon and in Southern Brazil a statistically insignificant brightening was observed, with significant contribution from decreasing biomass burning emissions in the former and competing minor contributions in the latter. These results can contribute to deepen the knowledge and understanding of SSR long-term trends and their causes in South America, reducing the underrepresentation of this continent when compared to regions like Europe.

1. Introduction

Decadal trends in surface solar radiation (SSR) have been the subject of study since pioneering studies in late 1980s and early 1990s made efforts to try to understand the long-term variation of SSR (Ohmura and Lang, 1989; Russak, 1990; Dutton et al., 1991; Stanhill and Moreshet, 1992). Several studies have followed presenting the trends and discussing their causes and potential consequences in several parts of the world (Wild, 2009), such as in Europe (e.g. Natsis et al., 2024; Kazadzis et al., 2018; Manara et al., 2016; Norris and Wild, 2007; Power, 2003), North America (e.g. Liepert 2002), China (e.g. Feng and Wang, 2019; Wang et al., 2015; Xia et al., 2007), Japan (e.g. Kudo et al., 2012) and New Zealand (Liley, 2009). Global dimming (negative trends in SSR) and brightening (positive trends in SSR) have been associated, in most of the cases, with changes in cloud cover (e.g. Stjern et al., 2008;

34 Augustine and Capotondi, 2022) and changes in aerosol loadings (e.g. Wild et al., 2021, Kambezidis et
35 al., 2012), with the dominant aspect depending on regional atmospheric and emission features.
36 However, many regions of the world are still underrepresented by such studies, mostly because of the
37 lack of observational high quality data in most of developing and least developed countries in contrast
38 to regions like Europe, North America or Eastern Asia. South America is an important region to be
39 mentioned in this context.

40 The lack of long-term SSR data in South America, reported by different authors (Ohmura,
41 2009; Gilgen et al., 2009), is the main cause for the absence of a long literature in the region. Still, a
42 few studies tried to assess SSR variability in South America. Ohmura (2009) presented and discussed
43 SSR decadal trends based on a few stations in Venezuela at the end of the 20th century. Schwartz (2005)
44 used astronomical extinction measurements to estimate clear-sky SSR trends at one astronomical
45 observatory in Chile during two decades (1978-1997). Yuan et al. (2021) and Jiao et al. (2023) used
46 machine learning methods to spatially interpolate SSR ground observations and reanalysis data and
47 used this approach to assess SSR decadal variability over the whole globe, including South America,
48 covering the second half of the 20th century and the first two decades of the 21st century. Da Silva et
49 al. (2010), de Jong et al. (2019) and de Lima et al. (2019) all assessed SSR variability in Brazil with a
50 focus on the potential for photovoltaic energy production. Zuluaga et al. (2021) and Raichijk (2012)
51 used sunshine duration to assess the SSR variability in Brazil for the last 2 to 4 decades of the 20th
52 century and the beginning of the 21st century. A similarity between most of these studies is the fact that
53 they had to rely on reanalysis, modeling data and indirect estimators of SSR (like sunshine duration),
54 with the only of the abovementioned studies that used ground observations being limited to a small
55 region in Venezuela. This leaves regions such as the densely populated southeastern Brazil or the highly
56 climate-relevant Amazon region without any direct assessment of the regional SSR long term
57 variability. Yamasoe et al. (2021) presented and discussed a SSR time series of fifty-six years (1961-
58 2016) measured in the city of Sao Paulo, and that is, to our knowledge, the longest and most detailed
59 analysis of directly observed SSR in South America. The studies referenced here apply different
60 methods, to different regions, in different periods, so it is hard to directly compare them. But, in general
61 terms, studies based on sunshine duration tend to indicate a brightening in Brazil after 1980s, while
62 studies using machine learning techniques and regional observational studies show a spatial
63 heterogeneity in the SSR trends in Brazil in the last few decades. All these studies provide different
64 pieces of information about SSR variability in this part of the world, however, none of them provide a
65 large scale assessment of the long term SSR decadal trends using ground observations of SSR, as done
66 for regions like Europe (e.g. Chiacchio and Wild, 2010; Pfeifroth et al., 2018), China (e.g. Yang et al.,
67 2018) or the United States (e.g. Long et al., 2009).

68 To try to tackle this gap in literature, we made use of the availability of SSR data from
69 automated meteorological stations from the Instituto Brasileiro de Meteorologia (INMET) from 2001
70 onwards to provide a large scale assessment of SSR decadal trends and underlying causes at the

71 beginning of the 21st century in the Brazilian territory, which covers approximately half of the South
72 American continent. The direct assessment of SSR long-term variability (using observed SSR) over
73 such a large area in South America represents a novel contribution from this work. The objective of this
74 study is to present the in-situ observed SSR decadal trends around Brazil in the first two decades of the
75 21st century and discuss their underlying causes. This is done at the regional level, rather than locally,
76 by selecting stations in strategic locations around the Brazilian territory and grouping them into station
77 composites. With this study we intend to help to reduce the under representativity of Global Dimming
78 and Brightening (GDB) studies in South America.

79 2. Data and methods

80 2.1 In situ SSR and cloud cover measurements

81 Surface solar radiation data for 32 of the 34 stations (see table 3, in annex) is collected and
82 controlled by the Instituto Nacional de Meteorologia (INMET) and was retrieved from the BDMEP
83 portal (available at: <https://bdmep.inmet.gov.br/> (last access 27 Oct 2023)). The stations were chosen
84 based on data availability in the regions of each composite used in this study (see section 2.4). The data
85 was retrieved at hourly time resolution. All data was tested at the hourly time scale for consistency
86 using the physical and extremely rare limits established by Long and Dutton (2002). None of the
87 INMET stations used in this study were reported to have major discontinuities in the records.
88 Nevertheless, we still applied the penalized maximal F test by Wang (2008) to verify the time series for
89 inhomogeneities. No homogeneity problems were identified in the stations used in this study.

90 The hourly values were further converted into daily means by simply averaging taking the
91 average of the 24 hourly values in a day. If one hourly value was missing (due to either lack of data or
92 removal during quality test) the one hourly value was filled linearly using the previous and next hours
93 and the daily value was the average of 24 hourly values (23 observed and 1 filled linearly). If more than
94 one hourly value was missing, the daily value was not calculated. In this way, daily values were always
95 the result of the average of 24 hourly values. Daily values were further converted into monthly values
96 by simply averaging the daily means within the same month. Monthly values were only calculated when
97 at least 70% of the days in a month were available. For example, 70% of the days of any April are
98 equivalent to 21 days. Therefore, if any April had 21 or more valid daily values, the monthly value
99 would be calculated as the average of all available daily values. On the other hand, if less than 21 days
100 had valid data, the monthly value would not be calculated. Further conversion from monthly to annual
101 values again occurred by simply averaging the 12 months. If one, two or three monthly values went
102 missing, the long term mean (mean for the whole period with available data) for that month would be
103 used instead, and the annual mean was still calculated. If more than three monthly values were missing,
104 then the annual value was not calculated. In this way, the annual value was always a result of 12 monthly
105 values, from which no more than 3 were filled with the long term mean. The averaging procedure from

106 daily to monthly, and from monthly to annual values reproduces similar methodologies used in previous
107 studies (e.g. Stjern et al., 2008; Manara et al., 2016).

108 The BSRN (Baseline Surface Radiation Network, Ohmura et al., 1998; Driemel et al., 2018)
109 station at Florianopolis was also used in this study. Its data was provided at 15-minute intervals. Data
110 from the station operated by the Instituto de Astronomia, Geofisica e Ciencias Atmosfericas of the
111 Universidade de São Paulo (IAG/USP), located in the city of Sao Paulo was also used. Data from this
112 station was provided as daily means. Both time series were also checked for consistency with the same
113 procedure applied to the INMET stations, at the hourly time scale for the BSRN station and at the daily
114 time scale for the IAG/USP station. Metadata for both stations did not report any discontinuities, and
115 the tests performed using the penalized maximal F test by Wang (2008) also did not indicate any
116 inhomogeneity in the time series. The SSR long term variability at the Sao Paulo station was previously
117 carefully analyzed by Yamasoe et al. (2021). This station also has the longest time coverage among all
118 of the stations used in this study: all the other stations only have data after 2000, while this stations has
119 available data from decades earlier. But we limited the analysis to the period with coverage of the other
120 stations because we intend to investigate the SSR variability at the regional level (composites) rather
121 than at the local level (individual station). The procedure to convert from sub-daily to daily averages,
122 from daily to monthly and from monthly to annual values at these two stations was the same as the
123 procedure used for the INMET stations.

124 Cloud cover data was also retrieved through the BDMEP portal from the INMET. The stations
125 were the same as used for the INMET SSR measurements with the addition of data from Florianopolis.
126 In Florianopolis, where the SSR data is originally from BSRN, the location of the SSR and the cloud
127 measurements differ by a few kilometers. Cloud cover data is collected from visual inspections at 00,
128 12 and 18 UTC and is provided in units of tenths (1/10) of cloud cover.. The daily cloud cover values
129 used in this study are a result of the average from the 12 and 18 UTC observations. This is equivalent
130 to 9 and 15 local time at most of the stations used in this study (8 and 14 for the westernmost stations).
131 At the Sao Paulo station, the diurnal cloud cover values are a result of hourly observations between 7
132 and 18 local time. Cloud cover data was converted into monthly and then annual values using the same
133 procedure as used for the SSR data. The cloud cover data is also used to calculate the Cloud Cover
134 Radiative Effect (CCRE), following the procedure described by Norris and Wild (2007). This variable
135 gives an estimation of the change in SSR produced by changes in cloud cover.

136 The SSR data described in this section is used to estimate the SSR trends presented in table 1,
137 and to calculate the fractional atmospheric column absorption (see section 2.4), which also has the
138 trends presented in table 1. The cloud cover data described in this section was used to estimate cloud
139 cover trends presented in table 1 and to apply one of the two methods for clear-sky identification used
140 in this study (see section 2.3).

141 **2.2 Satellite and reanalysis data**

142 To investigate Aerosol Optical Depth (AOD) variability, we used data from the CAMS
143 (Copernicus Atmosphere Monitoring System) reanalysis (Inness et al., 2019), provided by ECMWF.
144 This product has monthly time steps and spatial resolution of approximately 80 km, with temporal
145 coverage starting from 2003. Gueymard and Yang (2020) validated CAMS data using AERONET
146 stations from around the world, including South America and found that the reanalysis performs well
147 in comparison to in-situ aerosol observations, therefore being well suited for regional and global studies.
148 To assess the Aerosol Absorption Optical Depth (AAOD) at 500 nm we used data from the OMAERUV
149 aerosol algorithm from the Ozone Monitoring Instrument (OMI, Torres et al., 2007). The product is
150 provided at daily time resolution and 1-degree resolution, and is available from 2004 onwards. Due to
151 the frequent occurrence of missing daily values in the AAOD data from OMI (due to different aspects,
152 such as cloudy scenes), conversion from daily to monthly values was done only when at least two days
153 in a month were available. From monthly to annual values the conversion was only performed when at
154 least 11 of the 12 months had available data (missing month would be filled with long term mean, that
155 is, the mean for the whole period with data availability). We should also highlight that aerosol
156 absorption is a variable highly dependent on the spectral region, thus the absorption at 500 nm could
157 not be representative for the whole spectrum.

158 We also used shortwave radiative fluxes measured at the Top of the Atmosphere (TOA) by the
159 CERES (Cloud and Earth's Radiant Energy System, Doelling et al., 2013) instruments on board of the
160 satellites Terra and Aqua. The CERES-SSF product (Doelling et al., 2016), used in this study, provided
161 TOA shortwave fluxes at monthly time intervals and 1-degree spatial resolution, from 2000 onwards.
162 The same product also provided incoming shortwave radiative fluxes at the TOA, which was also used
163 in this study. The data from CERES was used to estimate fractional atmospheric column absorption
164 (see section 2.4).

165 Anthropogenic emissions were assessed using EDGAR (Emissions Database for Global
166 Atmospheric Research, Crippa et al., 2018). The data provides anthropogenic emission estimates at 0.1
167 degree spatial resolution and does not consider large scale biomass burning, land use change and
168 forestry (Crippa et al., 2018). This dataset was used, even though it does not include biomass burning,
169 because it provides information about aerosol emissions from all other sources, which are also relevant,
170 such as urban and industrial emissions. For this study we acquired the data in annual values and in units
171 of $\text{kg m}^{-1} \text{s}^{-1}$. The unit was further converted to $\text{kg grid}^{-1} \text{year}^{-1}$ (kg emitted for each 0.1 degree grid per
172 year). Finally, total column water vapour was obtained from the ERA5 reanalysis (Hersbach et al.,
173 2020), which provides data with a 0.25 degree spatial resolution and monthly time resolution. Cloud
174 cover from ERA5 was also used as supporting information in addition to the previously mentioned
175 SYNOP cloud cover, measured in-situ.

176 The AOD, AAOD, water vapor and anthropogenic emissions data described in this section were
177 used to identify the spatial distribution of the trends for these variables. The TOA incoming and
178 outgoing irradiance data described in this section was used to estimate fractional atmospheric column

179 absorption (see section 2.4). For all gridded data described in this section, the stations were sampled by
180 taking the grid box containing the station coordinates.

181

182 **2.3 Clear-sky SSR**

183 Time series of clear-sky SSR were derived using two different methods. At all stations we used
184 (1) the clear-sky method proposed by Correa et al. (2022), and at the stations with Synop cloud cover
185 data we also (2) derived clear-sky using cloud cover information. We applied both methods on the daily
186 time series. For the first method, we calculate station specific daily transmittance thresholds for every
187 month of the year. Days with transmittance lower than this threshold for the specific station in the
188 respective month are flagged as cloudy and removed. Days with transmittance above the thresholds are
189 flagged as clear-sky. As this method relies on the reduction of atmospheric transmittance under cloudy
190 conditions, its main weakness is associated with extreme aerosol events that could suddenly strongly
191 reduce transmittance. Thus this method is not well suited for the analysis of high frequency (interannual)
192 variability, but it has been shown adequate for assessment of long term trends (Correa et al., 2022).

193 For the second method, we simply used in-situ observations of cloud cover to identify cloudy
194 scenes. We set the threshold of cloud cover to two tenths (20%), where any day with cloud cover above
195 that was flagged as cloudy and removed. The choice of the cloud cover threshold represents a trade-off,
196 where low thresholds (say, 0%) would completely avoid any cloud signal but would also remove days
197 with low cloud occurrence, where the effects of cloud-free processes still dominate, and leave the time
198 series with very few valid values. For this reason, we allowed a higher threshold, assuming that on days
199 with such low cloud cover (0-20%) the cloud-free processes still dominate the signal of the SSR
200 variability.

201 In both methods, the removal of cloudy days results in clear-sky SSR time series with many
202 gaps. Thus, special care should be taken when converting from daily to monthly values and from
203 monthly to annual values. Monthly values were only calculated when at least two daily values were
204 available for the respective month. But before taking their average, each available daily value is
205 normalized to the 15th day of the month by multiplying the daily irradiance with a normalization factor.
206 This normalization factor is a result of the ratio between the TOA daily irradiance at the 15th day of the
207 month and at the day flagged as clear-sky. This is done to correct for the solar geometry at different
208 times of the month. From monthly to annual values the procedure is the same as done for all-sky SSR:
209 the calculation is done when at least 10 months are available, with missing values being replaced by
210 long term means. When less than 10 months are available, the annual means are not calculated.

211

212 **2.4 Fractional atmospheric column absorption**

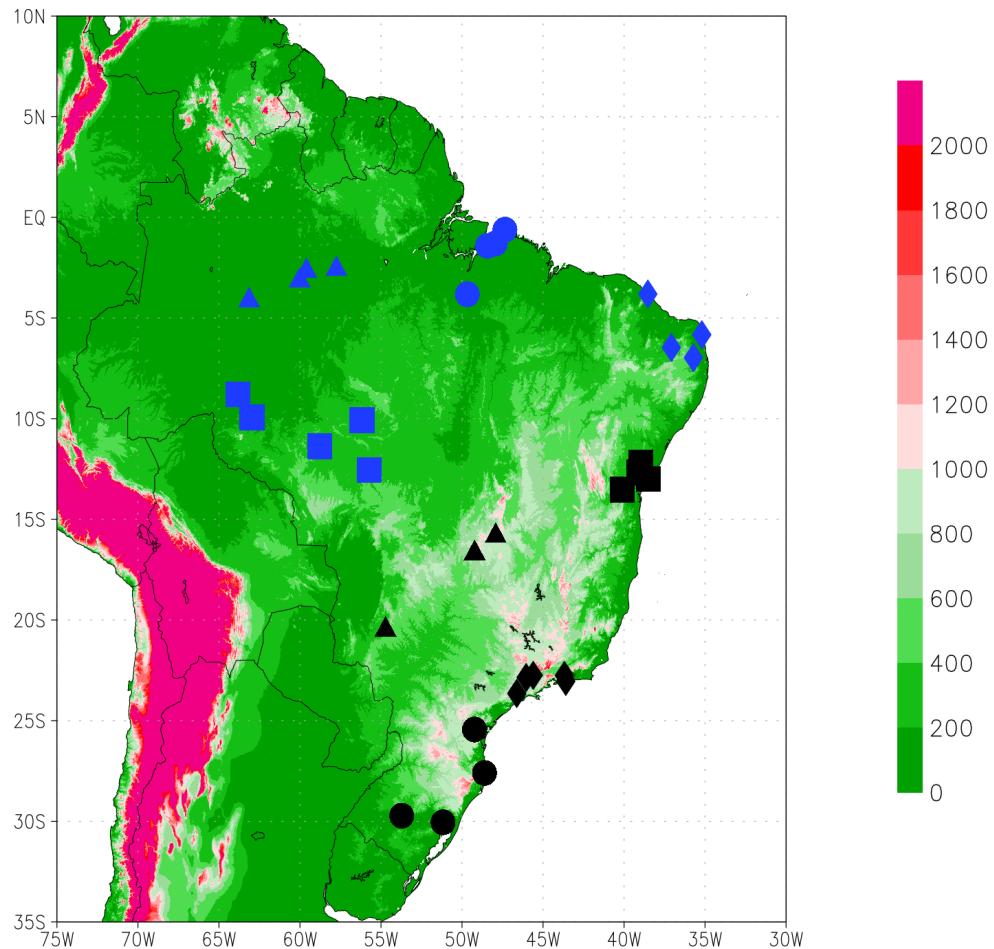
213 The daily fractional atmospheric column absorption (F_{abs}) was calculated for every station by
 214 combining SSR measured at the surface, surface albedo from ERA5 at the 0.25x0.25 degree spatial
 215 resolution and incoming and outgoing shortwave radiation at TOA from CERES-SSF 1deg from the
 216 Terra satellite (1x1 degree spatial resolution) and daily time resolution. For the gridded data the pixel
 217 containing the station coordinates was used. These variables were combined in equation 1 to calculate
 218 F_{abs} .

$$219 \quad F_{abs} = 1 - (SW_{upTOA}/SW_{downTOA}) - ((1-\text{albedo}_{SFC}) * (SW_{downSFC}/SW_{downTOA})) \quad (1)$$

220 SW_{upTOA} is the outgoing shortwave radiation at TOA, $SW_{downTOA}$ is the incoming shortwave
 221 radiation at TOA, albedo_{SFC} is the surface albedo and $SW_{downSFC}$ is the SSR. Thus, the term
 222 $(SW_{upTOA}/SW_{downTOA})$ represents the fraction (0-1) of the incoming shortwave radiation at the TOA
 223 which is reflected back to space, and the term $((1-\text{albedo}_{SFC}) * (SW_{downSFC}/SW_{downTOA}))$ represents the
 224 fraction (0-1) of the incoming shortwave radiation at the TOA which is absorbed at the surface. Then,
 225 F_{abs} represent the fraction of the incoming shortwave radiation at TOA which is absorbed within the
 226 atmosphere column. F_{abs} values can range between 0 and 1, where 0 would represent no atmospheric
 227 absorption and 1 would represent a black body absorption by the atmosphere.
 228

229 **2.5 Selection of station composites**

230 The stations used in this study were divided into eight composites based on geographical
 231 proximity, demographics and atmospheric features found in Brazil. That is, the composites were
 232 organized with the intent of covering different climate characteristics around the country and, in most
 233 cases, included data from big cities (> 1 million inhabitants). The use of data from big cities facilitates
 234 the construction of the composite time series, since the stations with longest time series and less missing
 235 data were found near big centers. The composites are: [1] Manaus region, [2] Belem region, [3]
 236 Fortaleza region, [4] Salvador region, [5] South Amazon, [6] Midwest Brazil, [7] Southeast Brazil and
 237 [8] South Brazil. The location of all stations are shown in Figure 1, and colors and markers denote the
 238 different composites. Each composite is composed of three to five stations. Based on literature review,
 239 Reboita et al. (2010) divided the precipitation regimes in South America in 8 regions, out of which five
 240 regions are in the Brazilian territory. Ferreira and Reboita (2022) revisited the topic and applied a non-
 241 hierarchical clustering technique to classify the precipitation regimes in South America. The authors
 242 also found 8 different precipitation regimes in the continent and only minor spatial differences to the
 243 previous study, with five of the regimes being present in the Brazilian territory. All of them were at
 244 least partly represented by the composites.



245
 246 **Figure 1: Map of Surface Solar Radiation stations and composites used in this study and topography of**
 247 **South America (in meters above sea level). Colors and shapes represent the different composites: Blue**
 248 **triangles = Manaus region; Blue circles = Belem region; Blue diamonds = Fortaleza region; Black squares**
 249 **= Salvador region; Blue squares = South Amazon; Black triangles = Midwest Brazil; Black diamonds =**
 250 **Southeast Brazil; Black circles = South Brazil.**

251 In the north of Brazil two composites were centered around the two biggest cities in the
 252 Brazilian Amazon, (1) Manaus and (2) Belem. Precipitation and cloudiness in both regions is strongly
 253 tied to local to mesoscale phenomena, like local convection, sea breeze circulation and squall lines. At
 254 the large scale, the Intertropical Convergence Zone (ITCZ) also has a significant influence on the
 255 precipitation in the regions, playing a major role for the seasonality of precipitation (Fisch et al., 1998).
 256 Feedbacks with the Amazon rainforest are also important, especially the recycling of precipitation. But
 257 regarding biomass burning in the Amazon, the most important area is located in the southern part of the
 258 Amazon (Artaxo et al., 2006), south of both Belem and Manaus. The occurrence of the South American
 259 Low Level Jet (Vera et al., 2006), important for moisture and aerosol transport from the Amazon to
 260 Southeastern Brazil, leaves the locations of Belem and Manaus with lower influence of biomass burning
 261 aerosols than the southern fraction of the Amazon. Still, the influence of aerosols from the forests (either

262 biogenic or biomass burning related) should not be neglected (Rosario et al., 2019), and most
263 importantly, the importance of anthropogenic emissions from such big population centers should be
264 taken into account.

265 In the northeast of Brazil, the composites of (3) Fortaleza and (4) Salvador share similar general
266 characteristics regarding precipitation and cloudiness regimes. The stations in these composites are also
267 centered around big population centers (Fortaleza and Salvador), where anthropogenic emissions
268 should be taken into account. The biggest difference to the composites around Manaus and Belem, is
269 that these two composites are not located in the Amazon region. But they are located in the same
270 precipitation regime division proposed by by Ferreira and Reboita (2022), with two stations of the
271 Fortaleza composite being located in a different subdivision.

272 The composite (5), South Amazon, was chosen to cover the region under the strongest influence
273 of biomass burning aerosols from the Amazon (Artaxo et al., 2006). The stations in this composite are
274 located in a different subdivision by Ferreira and Reboita (2022), where large scale phenomena (such
275 as the Bolivian high, the South Atlantic Convergence Zone and cold fronts) play an important role for
276 the cloud formation. This composite is not centered around a big city, and the most populated city in
277 the area is Porto Velho, with a population of approximately 500'000 people (IBGE, 2022). A few
278 degrees south of the South Amazon composite, are the stations of the (6) Middle West Brazil composite.
279 They are located approximately halfway between the South Amazon composite and the densely
280 populated Southeast Brazil. It is a dry region mostly influenced by large scale phenomena, compared
281 to the north and northeast regions of Brazil. The biggest city in the composite is Brasilia.

282 The Southeast is the most densely populated area in Brazil, where big centers like Sao Paulo
283 and Rio de Janeiro are located. Like the Middle West and South Amazon composites, cloud formation
284 in this region is mostly associated with large scale phenomena, with significant influence from local
285 convection and sea breeze being limited mostly to summer months (Reboita et al., 2010; Ferreira and
286 Reboita, 2022). The (7) Southeast Brazil composite covers this area. The transport of humidity and
287 aerosols from the south Amazon are both relevant aspects to consider. But regarding aerosols, urban-
288 industrial emissions from the large population centers should be more relevant. The last station
289 composite covers the Southernmost part of the country. The (8) South Brazil composite is entirely
290 located in subtropical latitudes, and covers its own precipitation regime subdivision from Ferreira and
291 Reboita (2022). Large scale phenomena like frontal systems and extra-tropical cyclones play a major
292 role for cloud formation and moisture transport from the ocean. It is also a densely populated region,
293 with big cities like Porto Alegre, Curitiba and Florianopolis, thus, urban-industrial aerosol emissions
294 should be taken into account.

295 The whole discussion in this study revolves around these eight composites. Each variable was
296 fully processed and converted to annual values at the station level, and only after that, they were grouped
297 with the other stations in the respective composite. The list of stations in each composite can be found
298 in Table 3 (in appendix).

299 **2.6 Trend calculations**

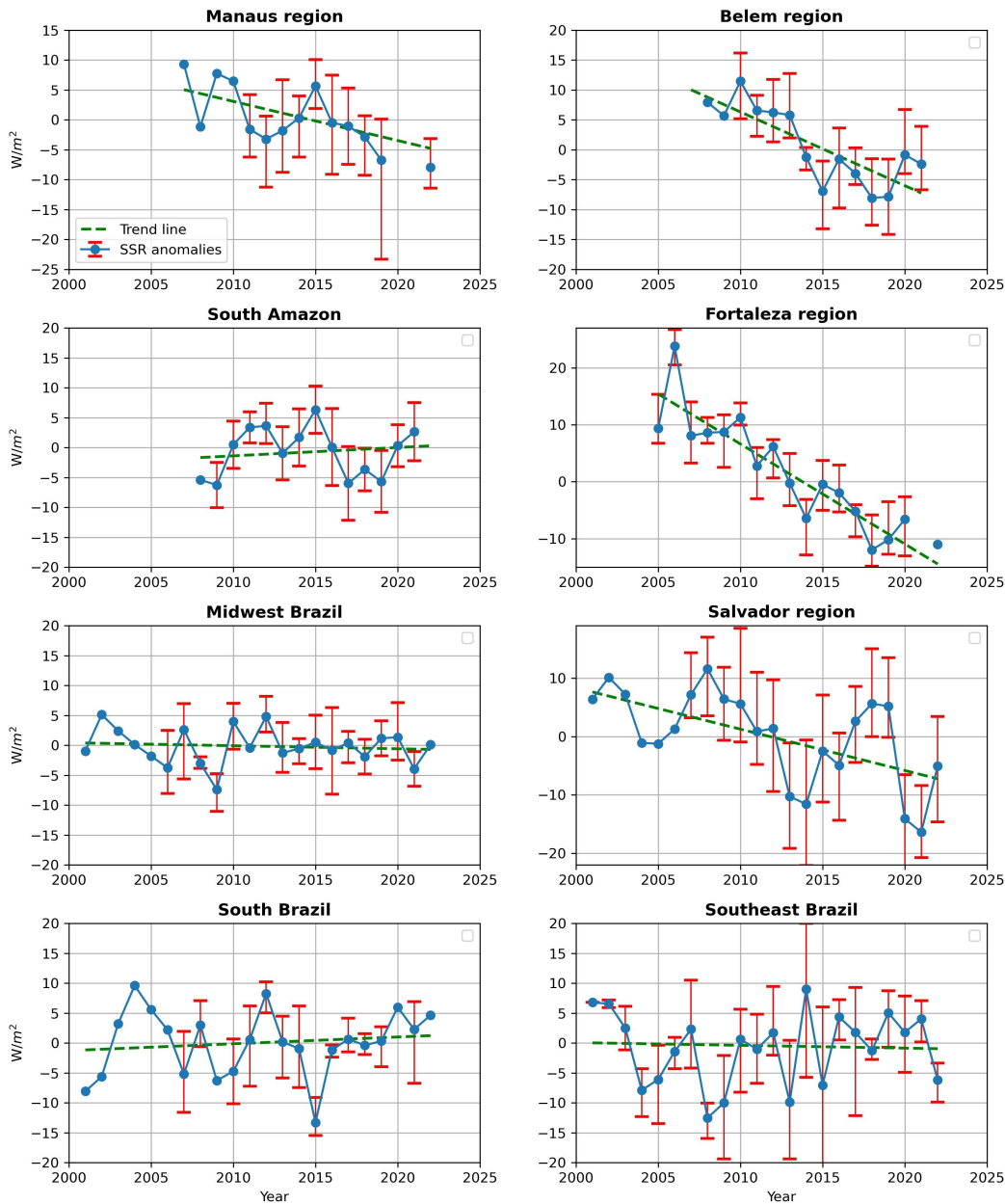
300 The trend analysis was based on annual anomalies of SSR. To calculate the annual anomalies,
301 the absolute SSR annual values were subtracted from the average SSR value for the whole period of
302 data availability for the respective composite (see table 1). This did not affect the trends, but facilitated
303 the visualization and comparison between time series, since the anomalies are centered around a
304 common value (zero). Decadal trends of SSR and most other variables presented in this study were
305 calculated using a Linear Least Squares (LLS) regression, with the confidence intervals (at the 95%
306 confidence level) being calculated using equation 4 from Nishizawa and Yoden (2005). Cloud cover
307 time series, in most cases, did not have the residuals normally distributed, thus, to account for that, we
308 calculated their trends using the Sen's slope (Sen, 1968) and Mann-Kendall test (Mann, 1945; Kendall,
309 1975). Trends of ground observations were calculated for the whole time availability of the composites,
310 however, as the time availability varies from one composite to the other, the periods used for trend
311 calculations vary by a few years. SSR trends are displayed in units of W/m^2 per decade. The period
312 considered in each composite is displayed in Table 1.

313

314 **3. Results**

315 **3.1 All-sky and clear-sky SSR trends**

316 Figure 2 shows the all-sky SSR anomalies time series of the 8 composites analyzed in this
317 study. All trends calculated in this study are shown in Table 1.



318

319

320

321

322

323

324

325

Figure 2: Time series of all-sky Surface Solar Radiation annual anomalies from the eight composites used in this study. Each composite is composed of three to five stations. In each composite, anomalies are with respect to the mean of the entire period (shown in table 1). The error bars indicate the maximum and minimum value for the individual stations in the respective year and composite. Trends are indicated by dashed lines.

Composites	Period	All-sky	Clear-sky (Correa et al., 2022)	Clear-sky (Synop)*	Synop Cloud cover	All-sky atm abs	Clear-sky atm abs	CCRE
Manaus region	2007-2022	-8.8 ± 4.2	-2.0 ± 2.3	-	1.2 [0.0; 2.0]	0.021 ± 0.007	0.005 ± 0.007	-1.1

Belem region	2008-2021	-11.7 ± 5.8	-4.8 ± 2.5	-	1.4 [0.4; 1.3]	0.016 ± 0.010	-0.001 ± 0.006	-1.5
Fortaleza region	2005-2022	-16.0 ± 4.2	-2.7 ± 1.8	-	0.8 [-1.3; 2.5]	0.034 ± 0.012	0.003 ± 0.011	-0.4
Salvador region	2001-2022	-7.0 ± 4.5	-3.7 ± 1.7	-	1.9 [0.7; 3.1]	0.016 ± 0.008	0.010 ± 0.006	-1.3
South Amazon	2008-2021	0.8 ± 6.4	1.6 ± 1.8	-	-	0.005 ± 0.015	-0.003 ± 0.007	-
Midwest Brazil	2001-2022	-0.4 ± 2.1	-1.8 ± 1.1	-2.5 ± 1.9	-1.3 [-2.1; -0.3]	0.005 ± 0.003	0.005 ± 0.005	1.4
Southeast Brazil	2001-2022	-0.1 ± 4.5	-1.6 ± 1.9	-7.7 ± 8.5	-3.7 [-5.5; -1.3]	0.002 ± 0.006	0.006 ± 0.007	3.9
South Brazil	2001-2022	2.0 ± 3.8	1.1 ± 4.1	1.2 ± 1.9	-0.2 [-1.3; 0.7]	0.001 ± 0.005	-0.003 ± 0.007	0.2

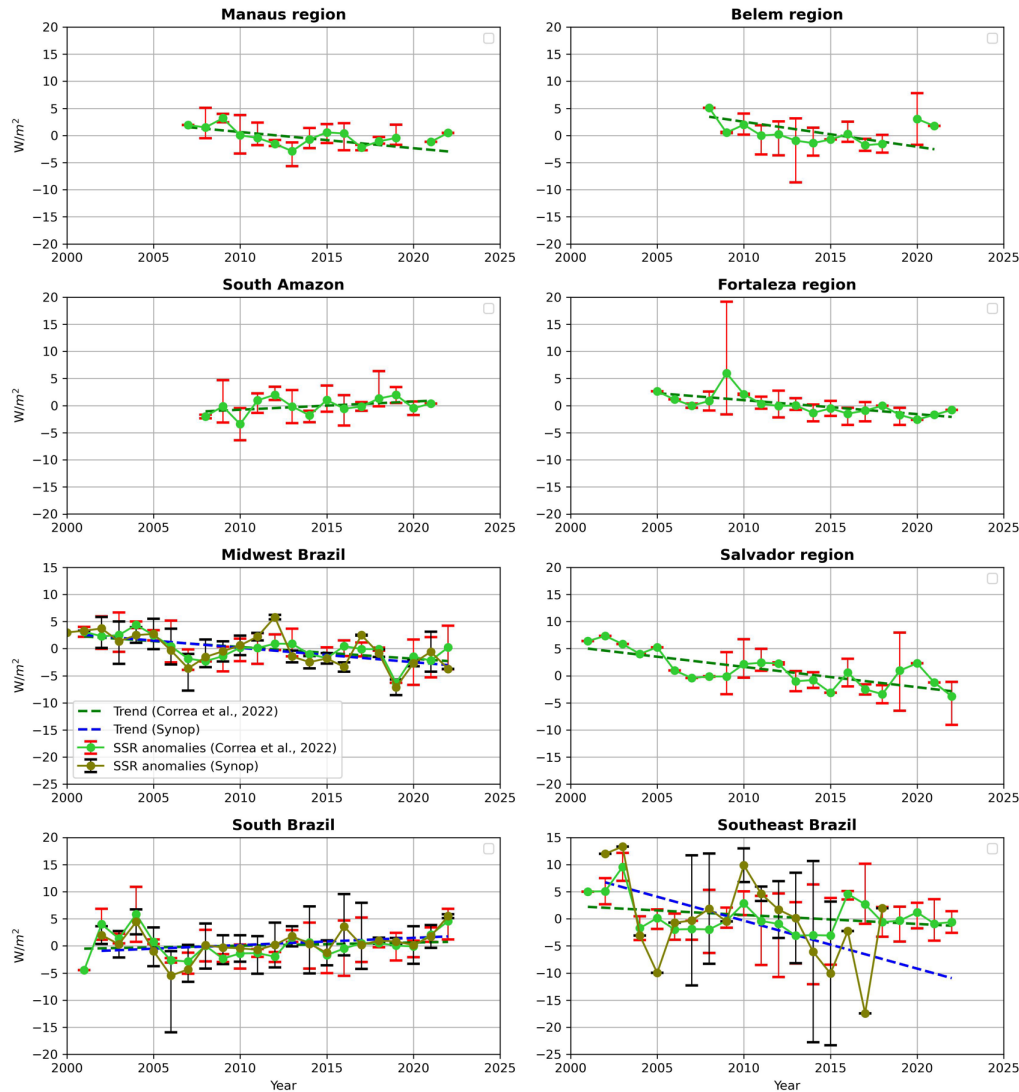
326
327
328
329
330
331
332
333
334
335
336
337
338
339
340
341

Table 1 - Trends (in W/m² per decade) for all-sky and clear-sky (using Correa et al., 2022, and using Synop cloud cover) SSR, all-sky and clear-sky (using Correa et al., 2022) fractional atmospheric absorption and Synop cloud cover at the 8 composites used in this study. Cloud Cover Radiative Effect (CCRE) referring to the Synop cloud cover trend also included - this is an estimate of the effect on SSR of the cloud cover changes. SSR trends in W/m² per decade; fractional atmospheric absorption trends in fraction (values between 0 and 1) per decade; Synop cloud cover in % per decade; and CCRE in W/m² per decade. Trends in bold are statistically significant at the 95% confidence level. Trends for Synop cloud cover were calculated using the Mann-Kendall test (see section 2.6), and as a result, the confidence interval is not always symmetrical. For this reason the confidence interval is shown in square brackets., Stations in each composite are listed in Table 3 (in appendix).

***Missing values for clear-sky Synop trends occur due to the limited amount of Synop cloud cover data (0 stations for the South Amazon composite, 2 out of 4 stations for Belem and Manaus composites) or due to not enough days flagged as clear-sky in order to generate a clear-sky time series (according to the procedure described in section 2.3).**

342
343
344
345
346
347
348
349
350
351
352
353
354

The period covered by the data in this study should always be kept in mind, as it is shorter than long-term studies of SSR trends in regions like Europe, North America and China. However, this timespan should be enough to start identifying the relevant features affecting SSR on timescales of a decade and beyond. In the North and Northeast Brazil composites (Belem, Manaus, Fortaleza and Salvador) statistically significant (at the 95% confidence level) negative SSR trends (dimming) were observed. In the Southeast and Middle West composites, trends were negative, although near zero and statistically insignificant. Southern Amazon and South Brazil composites both show statistically insignificant positive SSR trends (brightening). This reveals a contrasting spatial distribution of the all-sky SSR trends in the first two decades of the 21st century in Brazil: while strong dimming occurred in the northern half of the Amazon region and in the northeastern coastal region, near-zero to weak positive SSR trends occurred from the southern part of the Amazon down to the south of Brazil, including the central area of the country and the densely populated southeastern region. Figure 3 shows the time series of clear-sky SSR derived with the two methods used in the study.



355
 356 **Figure 3: Time series of clear-sky Surface Solar Radiation annual anomalies (with respect to the composite**
 357 **full time coverage, shown in Table 1) from the eight composites used in this study. Light green time series**
 358 **derived using the method by Correa et al. (2022) and olive green time series derived using Synop cloud**
 359 **cover to identify clear-skies. The error bars indicate the maximum and minimum value for the individual**
 360 **stations in the respective year and composite. Trends are indicated by dashed lines.**

361 Time series of clear-sky SSR based on synop cloud cover could not be derived in five out of
 362 the eight composites (see figure 3 and table 1). Synop clear-sky time series were derived when at least
 363 three stations in the composite had clear-sky data (see availability in table 3). The Manaus, Belem and
 364 South Amazon composites did not fulfill this requirement. For both Fortaleza and Salvador region
 365 composites, Synop cloud cover data was available for all stations, however, the few occurrences
 366 of low cloud cover days did not enable the derivation of clear-sky SSR time series
 367 following the procedure described in section 2.3.

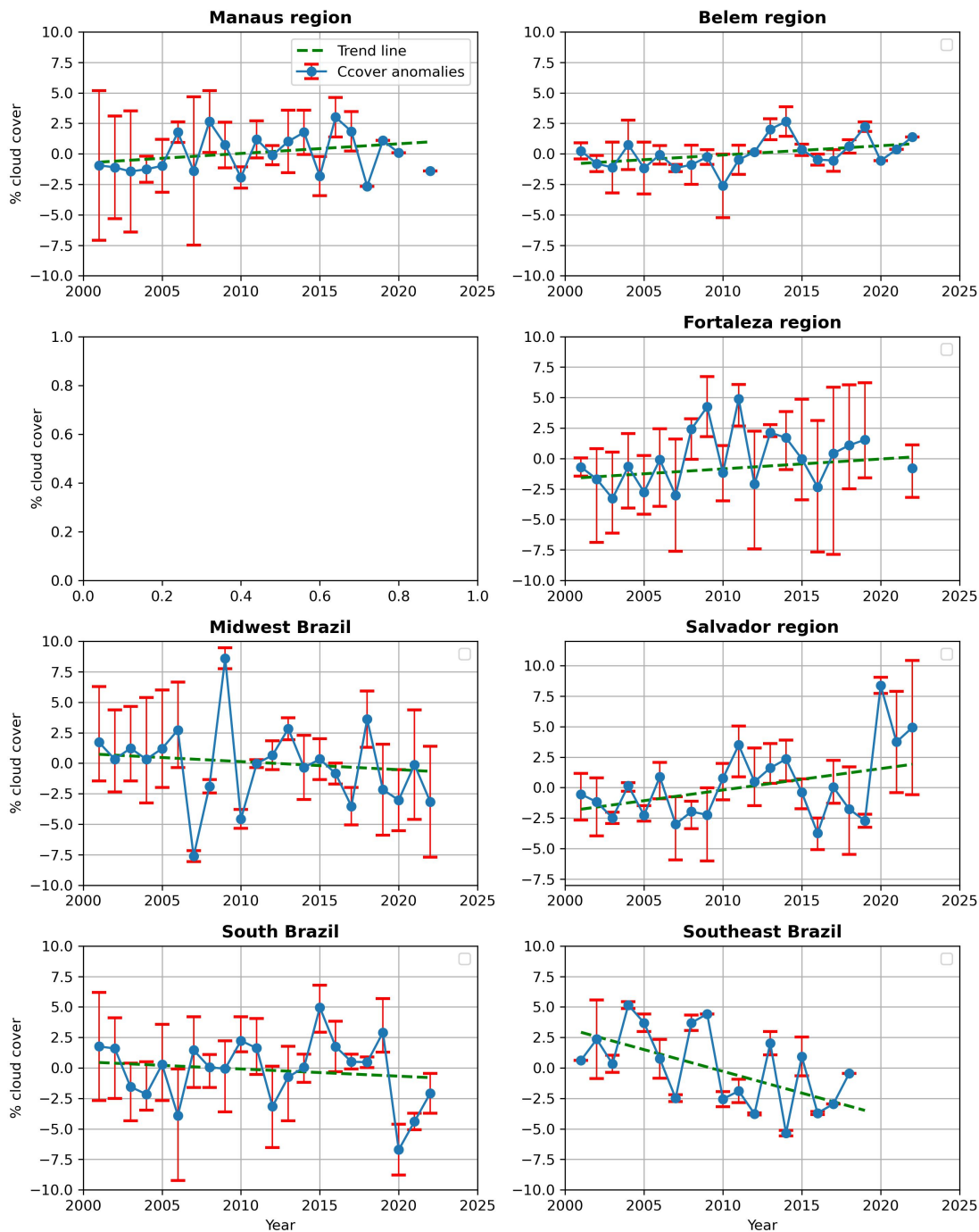
368 Clear-sky SSR time series show in general a similar pattern as observed in all-sky. All of the
 369 composites show the same sign as the trends in all-sky, and six of them also indicate the same statistical
 370 significance (or insignificance). The only exceptions are the Midwest and Manaus composites. The
 371 former showed statistically insignificant negative trends in all-sky SSR, but statistically significant

372 negative clear-sky SSR trends. The opposite occurred in the Manaus composite: statistically significant
373 all-sky SSR trends and statistically insignificant clear-sky SSR trends. For the composites where clear-
374 sky data could be derived with both methods, in two of them (South and Midwest Brazil) both methods
375 indicate very similar inter annual variability and trends, while in the other (Southeast Brazil) the two
376 methods do not show strong agreement in the inter annual variability, but agreed in the direction of the
377 trend. Therefore, the results of the clear-sky SSR trends are supported by both clear-sky methods.
378 Regarding the magnitudes of the clear-sky SSR trends in comparison to the all-sky trends, another
379 general pattern could be observed. In all composites with statistically significant negative all-sky SSR
380 trends (Belem, Manaus, Fortaleza and Salvador), the clear-sky SSR trends showed a substantially
381 smaller magnitude. In the Southeast and Middle West, both with near-zero all-sky SSR trends, the clear-
382 sky SSR trends were both negative and of larger magnitude than their all-sky counterparts. In the two
383 composites with observed statistically insignificant all-sky SSR brightening (South Amazon and South
384 Brazil), the clear-sky SSR trends showed similar magnitudes as the all-sky SSR trends.

385 These results indicate that the clear-sky processes in the atmosphere contributed to the observed
386 all-sky SSR trends in the whole of Brazil, but only in the Southern Amazon and in South Brazil their
387 magnitude might have been large enough to be able to explain the observed SSR trends. “Clear-sky
388 processes” in this context refers to the interaction between solar radiation and the components of the
389 atmosphere without the presence of clouds. Further analysis is thus needed to better understand the
390 reasons for the clear-sky and all-sky decadal SSR trends observed in Brazil.

391 **3.2 Cloud cover, AOD and water vapour trends**

392 Clouds, aerosols and water vapour all can attenuate solar radiation, therefore, their variability
393 is analyzed in more details in this section. The order in which they are mentioned follow the order of
394 relevance in the discussion of solar radiation attenuation in the atmosphere, with clouds being the most
395 important aspect and water vapour the least important aspect. Figure 4 shows the SYNOP cloud cover
396 time series for 7 of the 8 composites analyzed in the study (the cloud cover time series for the Southern
397 Amazon composite could not be constructed due to too much missing data). The associated trends can
398 be found in Table 1.



399

400

401 **Figure 4 - Time series of annual mean Synop cloud cover for seven of the eight composites used in this**
 402 **study. Not enough data was available to derive a time series for the South Amazon composite. The error**
 403 **bars indicate the maximum and minimum value for the individual stations in the respective year and**
 404 **composites. Trends are indicated by dashed lines.**

404

405

406

407

408

409

409

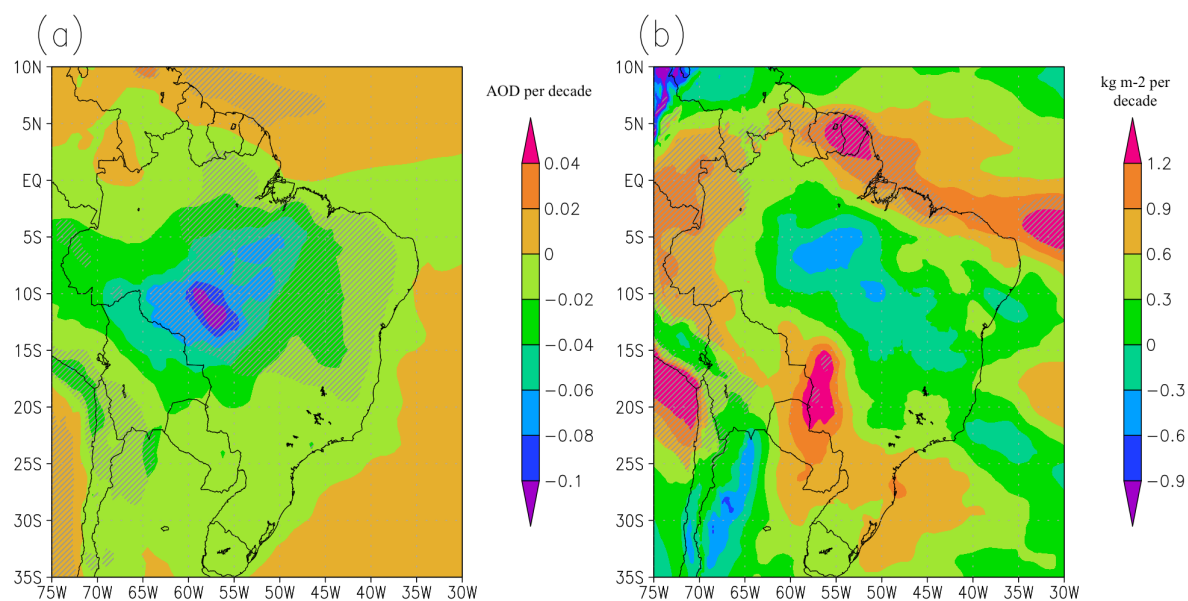
The Manaus, Belem and Southeast Brazil composites do not have synop cloud cover data for all stations (2 out of 4 available for Manaus and Belem, and 3 out of 5 for Southeast Brazil), therefore a comparison between all-sky SSR trends and Synop cloud cover at these composites is based on the assumption that the cloud cover observations for the composites are representative for all stations. This is a reasonable assumption given the geographical proximity between the stations within these three composites and the lack of any climatic or geographical feature that can strongly affect cloudiness at

410 individual stations (e.g. high topography). In these composites, all stations are located in areas with the
411 same precipitation regimes as classified by Ferreira and Reboita (2022), also corroborating with the
412 assumption of good representativeness.

413 Cloud cover trends are in most cases consistent in sign with the all-sky SSR trends. That is,
414 positive (negative) trends in cloud cover occurring during a period of negative (positive) SSR trends.
415 That is the case for the four composites with statistically significant all-sky SSR dimming (Belem,
416 Manaus, Fortaleza and Salvador). They all show positive trends in cloud cover, and all, except
417 Fortaleza, show statistical significance. This is consistent in the sense that the increase in cloud cover
418 contributes to the observed decrease in SSR, especially considering that the magnitude of the clear-sky
419 SSR trends at these locations was significantly smaller than the all-sky SSR trends. However,
420 quantitatively, the small magnitude of the cloud cover trends (between 0.8 and 1.9 % per decade)
421 challenges any hypothesis of a major contribution of cloud cover changes to the decadal SSR trends.
422 That is, the cloud cover trends are too small and, as a consequence, the contribution of changes in
423 cloud cover to the SSR trends is expected to be minor. This contribution is estimated objectively by the
424 CCRE (see table 1), which shows, in most cases, low values (in comparison to the all-sky SSR trends),
425 suggesting only a minor contribution from cloudiness to the SSR trends.

426 Cloud cover trends show near-zero values in the South region, suggesting no major cloud cover
427 contribution to the SSR trends. Southeast and Middle West show both statistically significant negative
428 trends in cloud cover, with remarkably strong values in SE (-3.7 [-5.5; -1.3] % per decade). Both
429 composites show near-zero but negative all-sky SSR trends, with stronger negative clear-sky SSR
430 trends. Thus, the cloud cover trends exert an opposite effect to the one of the clear-sky processes at both
431 composites. This is also consistent, in the sense that with clear-sky processes and cloud cover having
432 competing opposite effects, if their magnitude is similar, their effects cancel out, and the resulting all-
433 sky SSR trend would be near zero.

434 Figure 5 shows the decadal trend maps of annual AOD in the 2003-2020 period from CAMS
435 reanalysis and of total column water vapour in the 2001-2020 period from ERA5.



436
 437 **Figure 5 - Maps of decadal trends of (a) AOD [unitless] in the 2003-2020* period from CAMS reanalysis**
 438 **and of (b) total column water vapour [in kg m⁻²] in the 2001-2020 period from ERA5. Shaded areas indicate**
 439 **statistical significance (at the 95% confidence level).**
 440 ***The dataset was available only from 2003 onwards.**

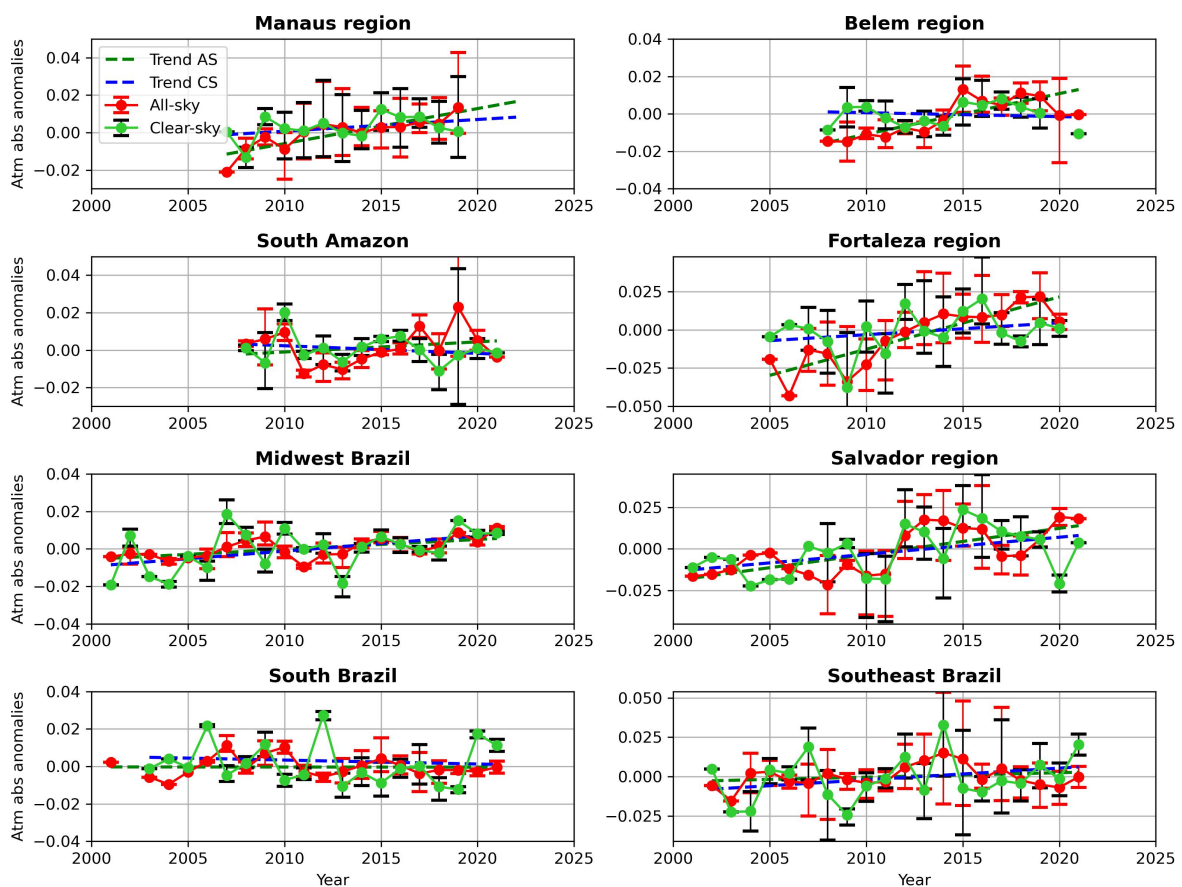
441 In Figure 5 (a) we see a strong negative AOD trend in the Southern Amazon in the period, and
 442 slightly negative to near-zero trends in the rest of the country. Trends are statistically significant in the
 443 Southern Amazon and in the inner area of the country down to approximately 15 degrees south (shaded
 444 areas), while they lose significance towards the coast. The process that dominates the AOD trends in
 445 the Southern Amazon (and in the whole country) is the reduction of biomass burning in the Amazon
 446 region. The Southern part of the Amazon region is the area that suffers most from the biomass burning
 447 (Artaxo et al., 2006), especially in the dry season during the southern hemisphere winter. A reduction
 448 in forest fires at the beginning of the 21st century has been reported (Silva Junior et al., 2021), and its
 449 effect is clear in the AOD trends. This result is consistent with the observed clear-sky SSR brightening
 450 in the Southern Amazon, but challenges the negative clear-sky SSR trends observed in most of the
 451 country. This suggests that changes in AOD were not primarily responsible for the clear-sky SSR trends
 452 in the whole of Brazil, with the exception of the Southern Amazon region.

453 The water vapour trend map (Figure 5 (b)) shows remarkably negative trends in the central
 454 Amazon, in a region around the east coast of Brazil and in the southernmost part of the country.
 455 Remarkably positive trends are present from the middle Western Brazil (south of the Amazon region)

456 stretching to Southeastern Brazil, and in the northeast and north coastal regions of the country. The
 457 spatial distribution of the decadal variability of water vapour does not generally comply with the
 458 observed clear-sky SSR trends. We used these trends to estimate the change in atmospheric clear-sky
 459 absorption due to solely water vapour, using the empirical model presented by Hakuba et al. (2016).
 460 Based on these estimations, even in a region with strong water vapour trend such as Midwest Brazil,
 461 these changes would be responsible for an increase in atmospheric clear-sky absorption (and
 462 consequently decrease in SSR) of approximately 0.4 W/m^2 per decade. This is almost one order of
 463 magnitude smaller than the clear-sky SSR trends in the region (-1.8 and -2.5 W/m^2 per decade, for
 464 clear-sky conditions based on Correa et al. (2022) and Synop cloud cover, respectively). This suggests
 465 that the water vapour contribution to the observed clear-sky SSR trends, when existed, was only minor.

466 3.3 Atmospheric absorption and Anthropogenic emissions

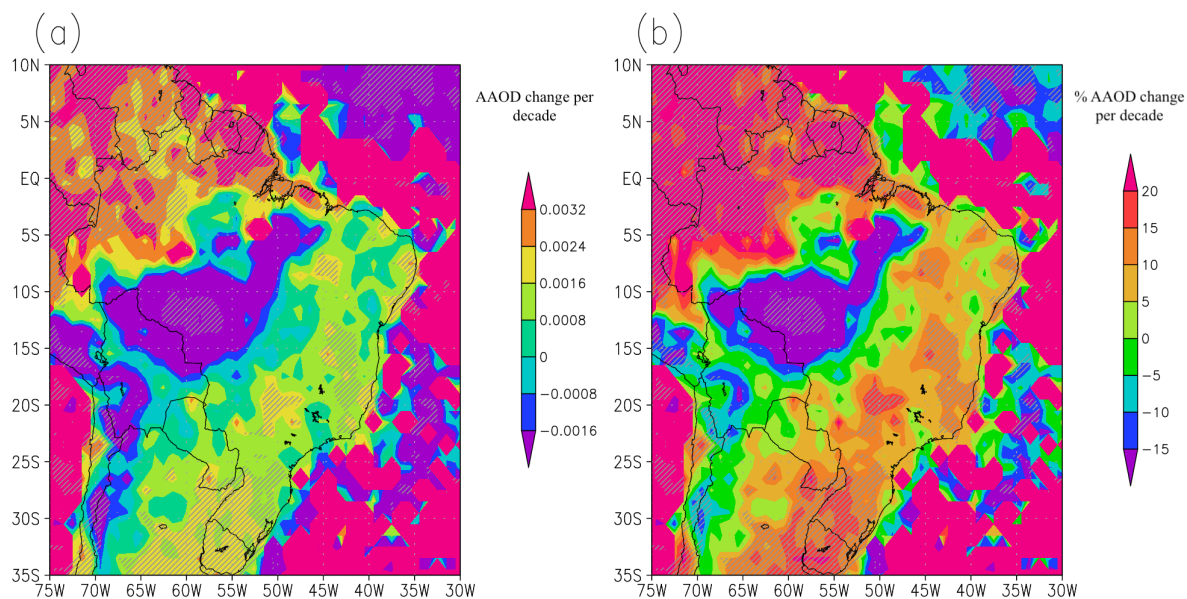
467 To better understand the reasons behind the observed clear-sky SSR trends and the overall
 468 processes responsible for the all-sky SSR trends, we analyzed the changes in fractional atmospheric
 469 absorption under all-sky and clear-sky conditions. This is a relevant aspect to be assessed, because
 470 changes in atmospheric shortwave absorption can be an important driver of SSR trends (Schwarz et al.,
 471 2020). Figure 6 shows these time series for the composites considered in this study both under all-sky
 472 and clear-sky conditions.



474 **Figure 6: Time series of all-sky (red) and clear-sky (green) fractional atmospheric column absorption**
475 **annual anomalies for the eight composites used in this study.**

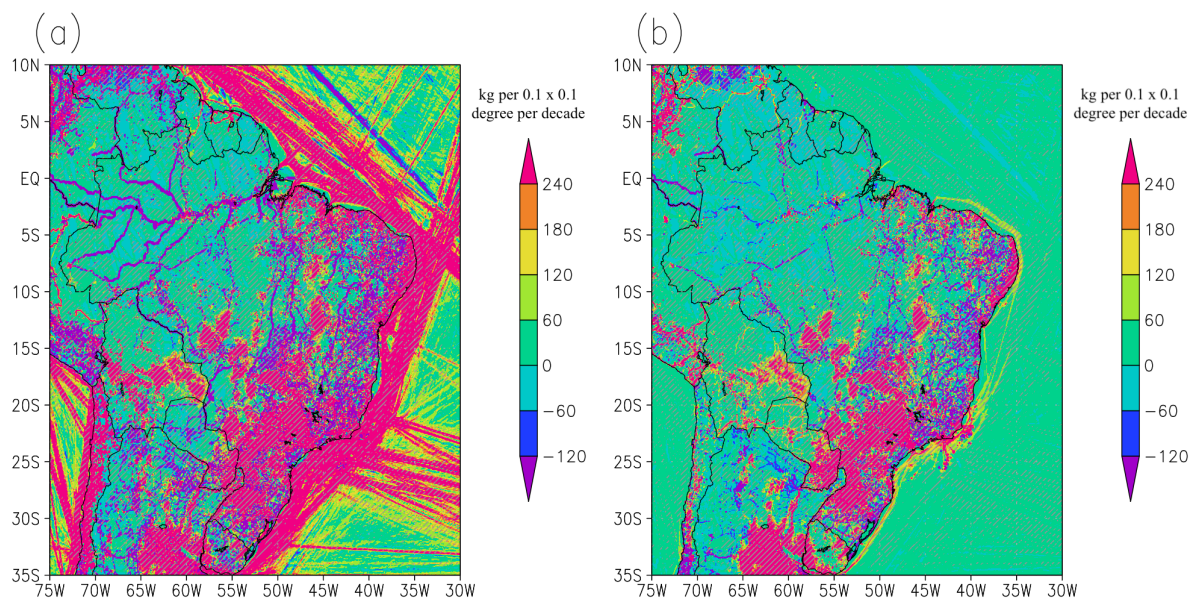
476 The fractional atmospheric absorption under all-sky conditions increased in most of the
477 composites in the first two decades of the 21st century. Five composites showed statistically significant
478 positive trends in F_{abs} , they are: Manaus, Belem, Fortaleza, Salvador and Middle West. The other
479 composites also showed positive trends, but they were statistically insignificant. Under clear-sky
480 conditions, the trends are obviously smaller, as the cloud induced multiple scattering does not play a
481 role in enhancing column absorption. Only in the Salvador and Middle West composites statistically
482 significant positive trends were observed in the atmospheric absorption under clear-sky conditions. All
483 the other composites show statistically insignificant trends with the same sign as their all-sky
484 counterparts, with the exception of the South Amazon, which shows statistically insignificant negative
485 trends under clear-sky, contrasting to a statistically insignificant positive trend under all-sky conditions.

486 These results reveal two important aspects of the SSR variability in Brazil. First, in seven out
487 of the eight composites the changes in clear-sky absorption comply with the clear-sky SSR trends. That
488 is, increasing (decreasing) clear-sky atmospheric absorption was always linked to a decrease (increase)
489 in clear-sky SSR. Secondly, the presence of clouds greatly increased atmospheric absorption (not
490 shown) but also its trends. This has most likely happened because of the intensification of multiple
491 scattering occurring under partially cloudy skies, resulting in a magnification of the trends seen in clear-
492 sky conditions. This is reinforced by the fact that the strongest all-sky atmospheric absorption trends
493 were found in the four cloudiest composites (Manaus, Belem, Fortaleza and Salvador), which happen
494 to be the four composites with statistically significant negative all-sky SSR trends (dimming). Even
495 though these results are consistent with each other, they also suggest that AOD only showed strong
496 trends in the South Amazon region, and that water vapour only contributed as a minor part to the
497 observed changes in atmospheric absorption (see discussion above). Thus, this raises the question of
498 what could be the main responsible for the changes in atmospheric absorption in Brazil. To try to answer
499 this question, we analyzed the decadal trend in aerosol absorption optical depth (AAOD) at 500 nm
500 from OMI. The trend map is displayed in Figure 7.



501
 502 **Figure 7: (a) Absolute and (b) relative (%) decadal trends in Absorption Aerosol Optical Depth (AAOD)**
 503 **in the 2005-2022 period from OMI. Shaded areas indicate statistical significance (at the 95% confidence**
 504 **level).**

505 The map shows a clear distinction between the region under strong influence of the forest fires
 506 in the Amazon (South Amazon) and the rest of Brazil. In the South Amazon, the data shows a decrease
 507 in AAOD in the 2005-2022 period, while in the rest of the country an increase in absorption AAOD at
 508 500 nm is observed. The spatial distribution of the trends suggests that the reduction in AAOD in the
 509 South Amazon could be associated with the forest fires reduction also visible in the AOD trends. In the
 510 whole rest of the country, positive trends in AAOD are observed. This reveals a significant change in
 511 the optical properties of the aerosols present in Brazil in the first two decades of the 21st century, with
 512 a trend towards more absorbing aerosols (at 500 nm) in most of the country. The AOD trend map
 513 (Figure 5a) shows that in the same areas where AAOD increases, AOD remains nearly constant, with
 514 trends close to zero. In order to better visualize potential reasons for an increase in AAOD at 500 nm
 515 in most of Brazil, we also investigated trends in anthropogenic SO₂ and Black Carbon emissions in
 516 Brazil. They are displayed in Figure 8.



517
 518 **Figure 8: Decadal trends of annual mean (a) SO₂ and (b) Black Carbon anthropogenic emissions (in kg per**
 519 **0.1x0.1 degree grid per decade) for the 2001-2018 period from EDGAR. Shaded areas indicate statistical**
 520 **significance (at the 95% confidence level).**

521 They show a general increase in anthropogenic emissions in most of Brazil, especially in highly
 522 populated areas. The only areas not showing increase in anthropogenic emissions are in the Amazon
 523 rainforest. This might be counterintuitive when comparing the emissions trends (figure 8) with AOD
 524 trends (figure 5a), as the strongest AOD trend is observed in the south of the Amazon region. However,
 525 EDGAR emission estimates do not consider large scale biomass burning, land use change and forestry
 526 (Crippa et al., 2018). As discussed in section 3.2, the AOD negative trend is mostly associated with
 527 reductions in biomass burning in the first two decades of the 21st century in the Amazon. Therefore,
 528 the biggest cause of the AOD trend (Figure 5a) is not considered in the emission data used in Figure 8.

529 Even though, according to figure 8, anthropogenic emissions did not increase significantly in
 530 the Amazon region, emissions still increased around the biggest cities in the region, like Manaus and
 531 Belem. This is of special relevance for this study, since seven of the eight composites are centered
 532 around cities with over a million inhabitants, where the large and usually increasing population (Lobo
 533 and Cunha, 2019) plays an important role to the atmospheric composition. The only composite that
 534 does not follow this rule is the South Amazon composite, where the biggest city is Porto Velho, which
 535 in 2020 had a population of less than 500'000 people (IBGE 2022). As anthropogenically emitted
 536 aerosols tend to account for a larger fraction of solar radiation absorption than natural aerosols (Wang

537 et al., 2009), this increase in anthropogenic emissions (especially of black carbon) complies with the
538 increasing AAOD in most of Brazil. Even though sulphate aerosols absorb much less shortwave
539 radiation than black carbon, the increasing presence of scattering aerosols can also have a similar effect
540 to the presence of broken clouds for atmospheric absorption (as discussed for the composites in North
541 and Northeast Brazil): they increase multiple scattering, increasing the optical path of the photons,
542 which increases the chances for absorption by the atmosphere. Therefore, the increasing anthropogenic
543 emissions complies with the observed increase in atmospheric absorption in most of Brazil in the period
544 of study. Similar results indicating a stronger impact of the changes in optical properties of the aerosols
545 than the changes in aerosol optical depth on the observed SSR trends were also found for Japan in the
546 1990s by Kudo et al. (2012).

547 **4. Discussion**

548 **4.1 Physical consistency of the results**

549 The results of this study point to a relevant impact of changes in atmospheric absorption in at
550 least half of the regions analyzed. However, this is based on the fractional atmospheric absorption data,
551 which is derived (as described in section 2.4) by combining in situ SSR (point) measurements with
552 gridded data of surface albedo and outgoing shortwave radiation at TOA, at 0.25 and 1.0 degree spatial
553 resolution, respectively. So the first question to be addressed is whether these results can be trusted
554 even with the use of different spatial resolutions. Schwarz et al. (2018) investigated the spatial
555 representativeness of SSR measurements in many stations around the world, including four stations in
556 Brazil: Florianopolis, São Martinho da Serra (both in South Brazil), Brasilia (in Middle West) and
557 Petrolina (~ 450 km away from Salvador). The authors found a good representativity of SSR for the 1-
558 degree surroundings at most stations around the world at the monthly time scales, with estimated
559 decorrelation lengths (the distance over which a point measurement is representative) always higher
560 than 3 degrees in all of the four Brazilian locations. Madhavan et al. (2017) investigated spatial
561 representativeness of SSR measurements at shorter time scales, and found that point measurements
562 were representative to a 10 x 10 km area in time scales up to around one hour (from 26 minutes at
563 overcast conditions to 70 minutes at broken clouds conditions). The authors demonstrated that the
564 decorrelation lengths increase linearly (on a log-log scale) with decreasing frequency (longer time
565 averaging). Following the results of the study by Madhavan et al. (2017), this would lead to
566 decorrelation lengths around the order of 100 km (~1 degree) at the daily (24-hour) time scales.
567 Therefore, based on the interpretation of these results, we can expect a satisfactory consistency in the
568 results from combining point measurements at the surface with 1-degree measurements at the TOA at
569 daily time scales, as done in this study. An in-depth analysis to estimate the decorrelation lengths at
570 daily time scales of each station goes beyond the scope of the study.

571 The performance of the gridded products used used in this study are discussed in their
572 respective documentations, referenced in section 2. Spectral surface albedo is reported as a main source
573 of uncertainty in the satellite based products, especially OMI AAOD, however, this tends to be a major
574 problem over the ocean. Sub-grid cloud contamination tends to also represent a problem for the retrieval
575 of satellite based products. But this is reported to lead to an over/under estimation of the average AAOD,
576 but should not affect the representation of its long-term variability. No issues with the long-term
577 variability of the reanalysis products were reported.

578 Regarding atmospheric absorption, previous studies (e.g. Li et al., 1995; Byrne et al., 1996)
579 have shown an enhancement in atmospheric absorption under cloudy conditions. According to previous
580 literature, such an enhancement would not be caused by cloud absorption, but by cloud scattering, which
581 increases the optical path of a photon in the atmosphere, consequently increasing the chances of this
582 photon to be absorbed by other components of the atmosphere, such as water vapour and aerosols. Even
583 though the existence of this mechanism is clear, the quantitative influence this could have on the energy
584 budget at any location would also depend on the characteristics of cloud occurrence (e.g. the frequency
585 of cloud free, overcast and partially cloudy conditions). As much as cloud free conditions are not
586 optimal for atmospheric absorption, completely overcast conditions are not either. Under fully cloudy
587 conditions, the backscattering of incoming shortwave radiation is high, usually not increasing the
588 optical path of the photons and not allowing them to reach lower levels of the atmosphere, where water
589 vapour and aerosol concentrations are higher. Thus, the high occurrence of partially cloudy conditions
590 would increase the cloud effects on atmospheric absorption, via the increase in the optical path of the
591 photons. Such conditions are found in Belem, Manaus, Fortaleza and Salvador, due to the importance
592 of local convection for cloud formation in such hot and humid locations. The differences in the
593 fractional atmospheric absorption trends between clear-sky and all-sky conditions at these locations
594 reinforces this: trends under all-sky conditions are one order of magnitude larger than their clear-sky
595 counterparts. This is not observed at all the other locations, which have a higher dependence on
596 mesoscale and synoptic scale phenomena for cloud formation than the previously mentioned locations.
597 In fact, a difference in the precipitation regimes between the region where all the four above-mentioned
598 composites are located and the rest of Brazil has already been pointed out by Reboita et al. (2010) and
599 by Ferreira and Reboita (2022).

600 Chtirkova et al. (2023) investigated the potential effect of internal variability on the SSR trends,
601 and the relevance especially of Atlantic oceanic modes like the Atlantic Meridional Mode (AMM) or
602 the Atlantic Multidecadal Oscillation (AMO) to affect SSR trends by changing cloudiness in Brazil.
603 The AMM and AMO went to lower values during the period of study (2001-2022), which should lead
604 to decreasing SSR in Northeastern Brazil. This is consistent with the negative SSR trends in the region.
605 But it is important to note that this reduction in the oceanic modes values did not represent a major
606 phase transitions of these modes. A major increase in AMO occurred in the 1990s, and the cloud cover
607 trends (from ERA5) for the 1990-2006 period show a strong decrease in cloud cover in most of Brazil,

608 especially the south and western part of the country. No SSR data was available for further investigation
 609 in this study, but the importance of internal variability for SSR trends should not be neglected in future
 610 studies

611 The trends in SSR and supporting information in the eight composites made it possible to
 612 separate the discussion of the causes for the SSR trends into three groups. The composites in each group
 613 and their common characteristics are listed on table 2.

Composites	Common characteristics
Manaus, Belem, Fortaleza and Salvador	Strong all-sky dimming
	Distinguished clear-sky dimming with lower magnitude than the all-sky
	Positive cloud cover trends
	Positive trends in all-sky atmospheric absorption
Southeast Brazil and Midwest Brazil	Positive trends in clear-sky atmospheric absorption, but one order of magnitude smaller than their all-sky counterparts (this item does not apply to Salvador)
	Strong negative cloud cover trends
	Negative clear-sky SSR trends
South Amazon and South Brazil	Negative and statistically insignificant SSR trends
	Statistically insignificant all-sky brightening
	Statistically insignificant clear-sky brightening

614

615 **Table 2: Groups of composites with and their common characteristics as indicated by the results**
 616 **presented in this study.**

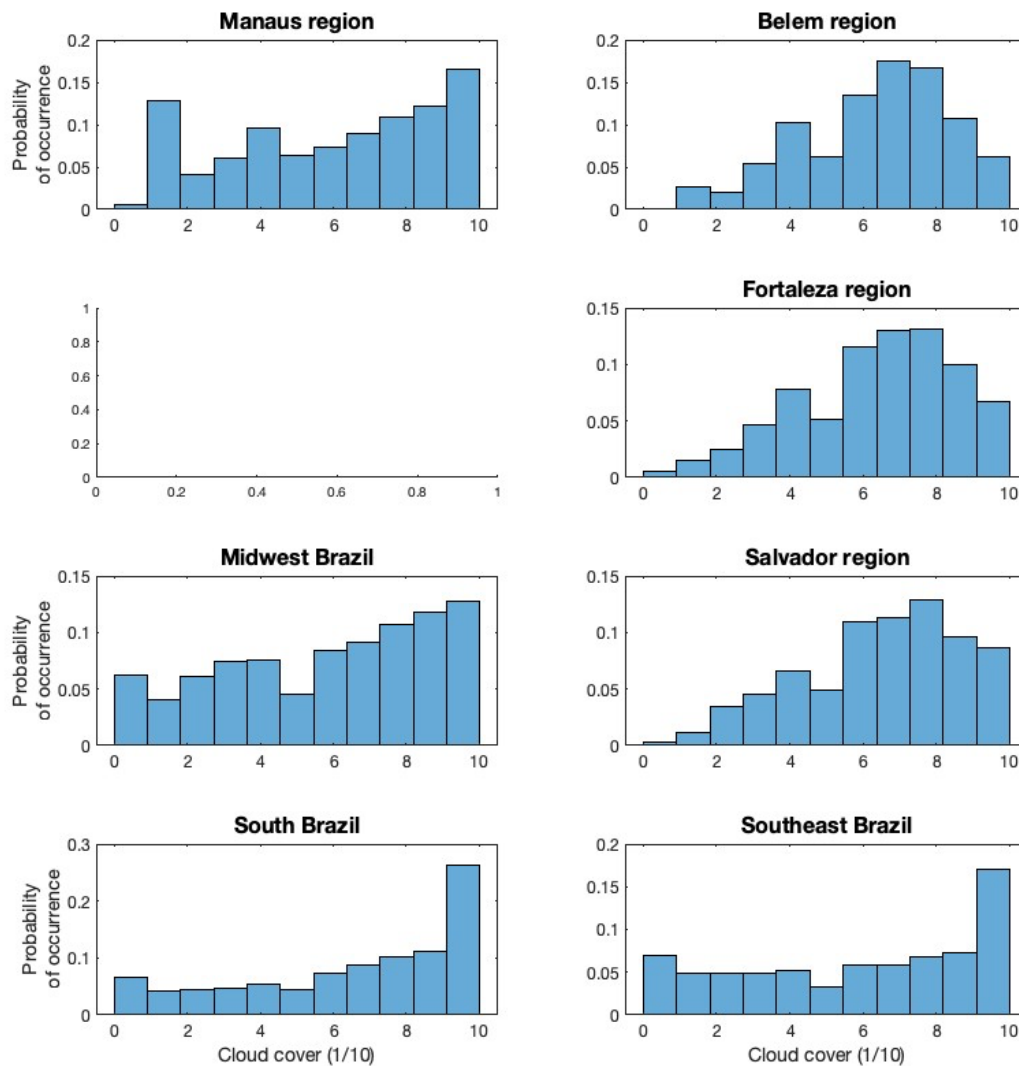
617 Based on this, we separated the discussion on the causes for SSR trends in three sections, each
 618 discussing one of the three groups.

619 4.2 Dimming in North and Northeastern Brazil

620 In this section, we discuss the dimming observed in the Manaus, Belem, Fortaleza and Salvador
 621 composites, located in North and Northeastern Brazil. All of the composites showed statistically
 622 significant all-sky dimming in the period, associated with a clear-sky dimming which was statistically
 623 significant in all composites, except Manaus. The difference in the magnitude of the all-sky SSR trends
 624 (from -6.3 W/m^2 per decade in Salvador to -18.8 W/m^2 per decade in Fortaleza) to the clear-sky SSR
 625 trends (from -2.0 W/m^2 per decade in Manaus to -4.8 W/m^2 per decade in Belem) in the four composites
 626 suggests that the clear-sky processes alone are unlikely to be strong enough to explain the SSR trends

627 in these locations. However, the fact that the clear-sky trends show the same sign as the all-sky trends,
628 with (in most cases) statistical significance, indicates that processes occurring under clear-skies did
629 contribute significantly to the overall trends. The contrast between all-sky and clear-sky also indicates
630 a potential contribution of changes in cloud cover to the trends. In fact, we identified positive cloud
631 cover trends, consistent with the observed reduction in SSR, but the magnitude of the trends (from 0.8
632 % per decade in Fortaleza to 1.9 % per decade in Salvador) and the resulting impact of these cloud
633 cover trends on the SSR trends, estimated by the CCRE (see Table 1), is small when compared to the
634 SSR trends. Thus, our results (summarised in the table 1) suggest contributions from both clear-sky
635 processes and cloud cover to the SSR trends, but none of them show a remarkable dominance compared
636 to the other.

637 Further analysis of the atmospheric absorption showed strong positive (and statistically
638 significant) trends in atmospheric absorption in all four composites. Schwarz et al. (2020) have shown
639 that changes in atmospheric shortwave absorption can be an important driver of dimming and
640 brightening. We also found that the atmospheric absorption trends were greatly enhanced by the
641 presence of clouds. This happens because the scattering by clouds increases the optical path of the
642 photons. This effect occurs primarily under broken clouds conditions, when three-dimensional multiple
643 scattering magnifies this effect. Our findings comply with the results presented by Byrne et al. (1996)
644 and references therein, which highlight the enhancement of atmospheric absorption of solar radiation
645 under broken clouds conditions. Results from Li et al. (1995) also suggested that this effect is stronger
646 in tropical regions, and the authors discuss that this is associated primarily aerosol and water vapour
647 absorption rather than cloud absorption. The characteristics of the distribution of cloudiness in the four
648 composites, displayed in Figure 9, might also play a role in this process. Stations from these composites
649 tend to have frequent occurrences of partially cloudy conditions. In the Belem, Fortaleza and Salvador
650 composites the daily cloud cover is between 25% and 80% in around two thirds of the days. For the
651 Manaus and Midwest Brazil composites this range of cloud cover occurred in around half of the days
652 and for South and Southeast Brazil composites this value is around one third. Thus, at the daily scale
653 we see a dominance of partially cloudy occurrences at three out of the four composites discussed in this
654 section. Even though the same distinguishable characteristic was not found for the Manaus composite
655 at the daily scale, based on the regionalization of precipitation regimes by Reboita et al. (2010), we
656 would expect the same finding at a more refined time scale also for the Manaus composite. That would
657 be the expectation because of the higher relevance of local convection at hot and humid locations
658 (convective clouds cause more broken cloud fields than large scale synoptic clouds) at the four
659 composites discussed in this section, in comparison to the other composites, where mesoscale and
660 synoptic meteorological systems tend to play a more important role for cloud formation. This higher
661 occurrence of broken clouds in the regions of the four composites discussed in this section then tends
662 to play an important role for the enhancement of atmospheric absorption.



663

664

665 **Figure 9: Distribution of daily Synop cloud cover occurrences in seven out of the eight composites used in**
 666 **this study. Not enough data was available to derive a distribution for the South Amazon composite.**

667

668

669

670

671

672

673

674

675

676

677

678

A simple multiplication between the incoming TOA radiation at each composite and the trends in fractional all-sky atmospheric absorption (shown in Table 1) reveals an estimated increase in all-sky atmospheric absorption from approximately $6 \pm 3 \text{ W/m}^2$ per decade in Belem up to $14 \pm 5 \text{ W/m}^2$ per decade in Fortaleza. If we assume that such an increase in atmospheric absorption is directly reflected in a reduction in SSR, we find that the effect of changes in atmospheric absorption under all-sky conditions have a higher effect than the estimated clear-sky SSR trends (see table 1) and the estimated effects of changes in clouds cover (see CCRE in table 1), and are more consistent with the magnitude of the observed all-sky SSR trends (presented in table 1). Thus, these results suggest that the increase in atmospheric absorption was the strongest contributor for the negative SSR trends observed in these four composites in north and northeast Brazil, with contributions also from changes in cloud cover. The difference in the all-sky and clear-sky absorption trends at these four composites indicates that clouds played an important role in the increasing in absorption, most likely by enhancing the optical path of

679 photons via multiple scattering under partially cloudy conditions. The results also suggest that these
680 changes in atmospheric absorption were greatly influenced by the changes in the optical properties of
681 the aerosols present in these regions. Our results showed the occurrence of increasing anthropogenic
682 emissions of SO₂ and black carbon, which did not seem to significantly change the AOD (possibly
683 because of its competing effects with the reduction of biomass burning emissions in South Amazon),
684 but increased the AAOD. This is most likely the cause for the increase in atmospheric absorption at the
685 four composites. All of this points to a relevant influence of anthropogenic factors to the SSR trends in
686 the first two decades of the 21st century in the regions around Manaus, Belem, Fortaleza and Salvador.
687 Remembering that these are all big cities with over a million inhabitants each, therefore this result could
688 be biased towards big population centers.

689 4.3 Midwest and Southeast Brazil

690 In this section we discuss the causes of the decadal SSR trends in the Middle West and
691 Southeast Brazil composites. Both all-sky SSR composites show near-zero trends, with -0.4 ± 2.7 W/m²
692 per decade in the Middle West and -0.6 ± 5.4 W/m² per decade in Southeast Brazil in the first two
693 decades of the 21st century. Both composites show clear-sky SSR dimming (statistically significant in
694 the Middle West and statistically insignificant in the Southeast) and statistically significant decrease in
695 cloud cover in the period. An increase in atmospheric absorption was also observed at these locations,
696 but the trends were substantially smaller than the trends observed in the four composites discussed in
697 the previous section. These results already suggest different physical processes playing a role in the
698 causes of SSR decadal trends in these regions.

699 The trends in fractional clear-sky atmospheric absorption in the two composites are similar to
700 each other (0.0051 ± 0.005 per decade in the Middle West and 0.0059 ± 0.007 per decade in the
701 Southeast) and are larger than the trends in three out of the four composites discussed in the previous
702 section. The clear-sky absorption trends are also larger than the all-sky absorption trends in the Middle
703 West and Southeast. This indicates a bigger relative relevance of the cloud-free processes for the SSR
704 trends in these two regions compared to the four locations previously discussed. This is reinforced by
705 the clear-sky SSR dimming at the two locations, and is also most likely associated with increasing
706 anthropogenic emissions, which lead to more absorptive aerosols, without significant change in AOD.

707 A comparison between the results of these two composites with the four composites in North
708 and Northeast Brazil supports the discussion regarding the impacts of broken clouds to the solar
709 atmospheric absorption and the distribution of cloud cover occurrences, presented in the previous
710 section. As discussed by Reboita et al. (2010) and by Ferreira and Reboita (2022), in the region from
711 Middle West to Southeastern Brazil a stronger influence of large scale synoptic meteorological systems
712 like cold fronts, South Atlantic Convergence Zone (SACZ) and the South American Low Level Jet
713 (SALLJ) contrasts with Northern and Northeastern Brazil, where local convection and circulation play
714 a more important role. This leads to different precipitation and cloudiness regimes between the

715 composites discussed in this section and in previous section. These regimes magnify the effects of
716 atmospheric absorption in the North and Northeastern Brazil, again fitting to the results by Li et al.
717 (1995), while not doing so in the rest of the country.

718 The results of these two composites also show a significant positive effect of changes in cloud
719 cover on the SSR trends. Strong significant negative trends in cloud cover were observed at both
720 regions. As a result of the competing effects between cloud-free processes and changes in cloud cover,
721 the resulting SSR trends in the first two decades of the 21st century were negative, but near-zero, for
722 both composites. This shows opposing effects of anthropogenic (changes in aerosols) and natural
723 (changes in cloud cover) changes canceling out.

724 4.4 South Amazon and South Brazil

725 In this section we discuss the causes for the SSR decadal trends in the South Amazon and South
726 Brazil. In both regions statistically insignificant brightening was observed in the all-sky SSR trends.
727 Clear-sky SSR trends also showed brightening (statistically insignificant) in both regions. Cloud cover
728 trends in South Brazil were rather small (-0.4 [-1.4 ; 0.6] % per decade), while cloud data was not
729 available for South Amazon.

730 For the South Amazon, the most relevant aspect to be discussed is the strong negative trend in
731 AOD observed in the study period, associated with the documented reduction in deforestation and
732 biomass burning in the Amazon (Silva Junior et al., 2021). Amazon biomass burning aerosols play an
733 important role in the atmospheric transmissivity in the region, but their emission, and consequently their
734 effects, are highly seasonally dependent, as shown by Schwarz et al. (2019). For this reason, even
735 though the annual AOD decadal trends show very strong negative values, the strong effects on SSR are
736 present mostly in the dry season (southern hemisphere winter), and are smoothed out with annual means
737 and decadal trends calculations. The seasonal clear-sky SSR trends in this composite are positive
738 (statistically insignificant at the 95% confidence level) in winter and spring (5.0 ± 5.6 and 1.1 ± 3.9
739 W/m^2 per decade, respectively) and negative (statistically insignificant at the 95% confidence level) in
740 summer and fall (-2.6 ± 2.7 and -1.6 ± 3.3 W/m^2 per decade, respectively), reinforcing this hypothesis.
741 This smoothing of the AOD effects in the annual means and decadal trends is most likely the reason
742 why, despite the strong negative AOD trends in the region, the all-sky and clear-sky SSR trends show
743 positive trends with an absolute magnitude remarkably smaller than the trends observed in north and
744 northeastern Brazil. This counterintuitive result (strong negative AOD decadal trend not resulting in
745 strong brightening neither in all-sky nor in clear-sky SSR) reveals the importance of taking seasonality
746 into account when investigating the response of SSR to changes in AOD.

747 In South Brazil, the SSR decadal trends are weakly positive, not of statistical significance, both
748 under all-sky and clear-sky conditions. This suggests the lack of a strong driver for the SSR trends in
749 the period analyzed. Cloud cover shows a small negative trend (statistically insignificant). Near-zero
750 trends are also found in AOD and in atmospheric absorption. The map of AAOD at 500 nm shows small

751 positive trends in the period, but water vapour shows small negative trends. It is important to note that
752 due to the logarithmic response of atmospheric absorption to changes in water vapour (e.g. Hakuba et
753 al., 2016), this is the region in Brazil with the expected strongest sensitivity to changes in water vapour.
754 Combining all these results together denotes competing small effects from different sources, and this is
755 most likely the reason for the resulting non significant trend observed. Another relevant aspect to be
756 highlighted, is that the period of analysis did not show a strong transition in the signal from oceanic
757 modes in the Atlantic. Chtirkova et al. (2023) pointed out the importance of the AMM and AMO
758 oceanic modes for the SSR trends in South America. This could be relevant for all composites, but the
759 lack of strong effects on SSR changes of the existing forcing elements in South Brazil in the post 2000
760 period let us to hypothesize that in a transitional period of AMM and/or AMO, internal variability could
761 dominate the SSR trends in this region, especially via changes in cloud cover. This hypothesis is
762 reinforced by the cloud cover trends from ERA5 for the 1990-2006 period (Figure A1, in appendix),
763 which show strong negative cloud cover trends in the region associated with the transitioning of the
764 AMO from a negative to a positive phase. The expectation is that the cloud cover trends in this period
765 dominated the SSR trends, causing brightening in the last decade of the 20st century in South Brazil.
766 However, the lack of SSR data before 2000 did not allow us to verify this hypothesis.

767 5. Conclusions

768 In this study we presented and investigated the magnitudes of the SSR trends and their
769 associated causes over the first two decades of the 21st century based on 34 stations in Brazil, divided
770 into 8 composites of 3 to 5 stations each. These are: Manaus region, Belem region, South Amazon,
771 Fortaleza region, Middle west, Salvador region, Southeast Brazil and South Brazil. The exact temporal
772 coverage of the SSR time series was composite-dependent, covering 22 years (2001-2022) in the four
773 southernmost composites (South, Southeast, Middle West and Salvador), and only 14 years (2008-
774 2021) in the South Amazon composite, the shortest time spam of all composites in this study. The
775 limited length of the periods should be kept in mind, as they are shorter than the long-term
776 dimming/brightening studies performed in regions like Europe.

777 We used cloud cover data from in situ measurements, clear-sky SSR time series derived with
778 two different methods (using Synop cloud cover and using the method by Correa et al., 2022),
779 atmospheric absorption calculated combining in situ and satellite measurements, AOD from the CAMS
780 reanalysis, AAOD from OMI satellite observations and anthropogenic emissions from EDGAR to
781 investigate the causes of the SSR trends in the eight composites in their period of data availability. All
782 in-situ data went through quality control procedures to attest their validity and documentation of gridded
783 data was carefully considered to account for potential issues. Our results showed that a strong dimming
784 occurred in the composites located in north and northeast Brazil (Manaus, Belem, Fortaleza and

785 Salvador) in the period of study, while the other four composites all showed statistically insignificant
786 trends (positive in the South Amazon and South Brazil, and negative in the Southeast and Midwest).

787

788 A detailed ~~deeper~~ analysis ~~on the causes of the trend~~ on the data revealed significant
789 contributions of both clear-sky SSR and cloud cover changes to the trends observed in the north and
790 northeast Brazil, but with a dominance of the effects of increasing atmospheric absorption under all-
791 sky conditions. This is believed to be associated with increased anthropogenic/urban emissions, which
792 would also explain the clear-sky SSR dimming, and the characteristics of cloud occurrence in those
793 regions. Previous studies (e.g, Li et al., 1995; Byrne et al., 1996) have discussed the increase in
794 atmospheric absorption under broken cloud conditions due to the multiple scattering by clouds and
795 absorption by water vapour and aerosols. ~~In the case of north and northeast Brazil, we believe that this~~
796 ~~is associated with an increase in absorption possibly by aerosols, also responsible for a clear sky SSR~~
797 ~~dimming, and the characteristics of cloud occurrence in those regions.~~ The massive occurrence of
798 partially cloudy conditions at these regions, in comparison with the other composites analysed in this
799 study, make this mechanism much more relevant at the North and Northeast Brazil stations than in all
800 of the others. The importance of changes in atmospheric shortwave absorption to dimming and
801 brightening have also been highlighted by Schwarz et al. (2020). Even though in the present study we
802 have been able to identify different factors significantly affecting SSR trends in these regions and their
803 magnitude, future work would be important to more precisely quantify the contributions of each factors
804 causing SSR changes and to project the contributions of these factors in the future.

805 In Southeast and Middle West Brazil, statistically insignificant negative SSR trends in the
806 period indicated that no single strong forcing dominated dimming and brightening. ~~were most likely~~
807 ~~the~~ Therefore, the small trends were most likely the results of competing effects of negative cloud cover
808 trends (resulting in a positive forcing on all-sky SSR) and negative clear-sky SSR trends (resulting in a
809 negative forcing on all-sky SSR), where the clear-sky trends are also most likely associated with
810 changes in aerosol absorption (due to changes in anthropogenic/urban aerosols). In the South Amazon
811 the signal of the strong aerosol reduction, resulting from the reduction in biomass burning in the
812 Amazon at the beginning of the 21st century (Silva Junior et al., 2021), dominated the observed
813 brightening. This AOD reduction covered a large area in central Brazil, but did not reach most of the
814 other composites, and areas with the strongest negative AOD trends (stronger than -0.06 per decade)
815 were all located in the South of the Amazon. ~~But~~ However, the resulting SSR trends (both all-sky and
816 clear-sky) ~~were~~ not statistically significant. A potential reason for this might be the strong seasonality
817 of the biomass burning in the Amazon (Schwarz et al., 2019), which means that the strong changes in
818 AOD are affecting SSR only a few months per year, during winter and spring months (which might not
819 be massively relevant since the stations in the composite are around 10-15 degrees south). Due to
820 missing data we were not able to assess the extent of cloud cover contribution to this result. Finally in

821 South Brazil, competing minor effects of cloud-free processes and cloud cover changes resulted in
822 statistically insignificant brightening.

823 This study contributes to the understanding of the causes of SSR decadal trends in a world
824 region with still limited observational data. Further research would, however, be largely relevant,
825 especially in the quantification of each of the factors causing SSR changes and in the estimation of these
826 factors in the future.,~~and opens space for further research on the climate effects of such trends.~~

827 **Data availability**

828 The data from the IAG/USP station can be requested at
829 http://www.estacao.iag.usp.br/sol_dados.php (last access: 21 Feb 2024). The data from
830 INMET stations can be requested at <https://bdmep.inmet.gov.br/> (last access: 21 Feb 2024).
831 The BSRN SSR data is available at the BSRN website (<https://bsrn.awi.de/>). The CERES
832 products are available at the CERES website (<https://ceres.larc.nasa.gov/data/>). The ERA5
833 reanalysis data used in this study is available under
834 [https://cds.climate.copernicus.eu/cdsapp#!/dataset/reanalysis-era5-single-levels-monthly-](https://cds.climate.copernicus.eu/cdsapp#!/dataset/reanalysis-era5-single-levels-monthly-means)
835 [means](https://cds.climate.copernicus.eu/cdsapp#!/dataset/reanalysis-era5-single-levels-monthly-means) . The CAMS AOD reanalysis data is available under
836 <https://www.ecmwf.int/en/research/climate-reanalysis/cams-reanalysis> . Data of
837 anthropogenic emissions estimates is available at the EDGAR website
838 (https://edgar.jrc.ec.europa.eu/emissions_data_and_maps , last access: 21 Feb 2024). The data
839 from the OMI instrument used in this study is available at
840 https://disc.gsfc.nasa.gov/datasets/OMAERUVd_003/summary (last access 21 Feb 2024). The
841 satellite cloud fraction data from CLARA, used to apply the clear-sky method used in this
842 study, can be found on the CM SAF website (<https://www.cmsaf.eu/>) and downloaded using
843 the Web User Interface at <https://wui.cmsaf.eu/>

844 **Author contributions**

845 LFC designed the study, organised the data and wrote the original manuscript. DF, BC and MW revised
846 and edited the text. All authors contributed to the analysis and to the final paper.

847 **Competing interests**

848 The authors declare that they have no conflict of interest.

849 **Acknowledgements**

850 This study was funded by the Swiss National Science Foundation grant no. 200020_188601.
851 The authors would like to thank the Instituto Nacional de Meteorologia (INMET) and the Weather
852 Station of the Institute of Astronomy, Geophysics and Atmospheric Science of the University of São
853 Paulo for providing the meteorological observations. We express our gratitude to the teams that produce
854 and maintain the high quality meteorological data used in this study, from BSRN, CERES, ERA5,
855 CAMS, OMI, EDGAR and CLARA.

856 **References**

- 857 Artaxo, P., Oliveira, P. H., Lara, L. L., Pauliquevis, T. M., Rizzo, L. V., Junior, C. P., ... &
 858 Correia, A. L. (2006). Efeitos climáticos de partículas de aerossóis biogênicos e
 859 emitidos em queimadas na Amazônia. *Revista brasileira de meteorologia*, 21(3a),
 860 168-22.
- 861 Augustine, J. A., & Capotondi, A. (2022). Forcing for multidecadal surface solar radiation
 862 trends over Northern Hemisphere continents. *Journal of Geophysical Research:*
 863 *Atmospheres*, 127(16), e2021JD036342.
- 864 Byrne, R. N., Somerville, R. C. J., & Subaşilar, B. (1996). Broken-cloud enhancement of
 865 solar radiation absorption. *Journal of Atmospheric Sciences*, 53(6), 878-886.
- 866 Chiacchio, M., & Wild, M. (2010). Influence of NAO and clouds on long-term seasonal
 867 variations of surface solar radiation in Europe. *Journal of Geophysical Research:*
 868 *Atmospheres*, 115(D10).
- 869 Chtirkova, B., Folini, D., Correa, L. F., & Wild, M. (2023). Internal variability of the climate
 870 system mirrored in decadal-scale trends of surface solar radiation. *Journal of*
 871 *Geophysical Research: Atmospheres*, e2023JD038573.
- 872 Correa, L. F., Folini, D., Chtirkova, B., & Wild, M. (2022). A Method for Clear-Sky
 873 Identification and Long-Term Trends Assessment Using Daily Surface Solar
 874 Radiation Records. *Earth and Space Science*, 9(8), e2021EA002197.
- 875 Crippa, M., Guizzardi, D., Muntean, M., Schaaf, E., Dentener, F., Van Aardenne, J. A., ... &
 876 Janssens-Maenhout, G. (2018). Gridded emissions of air pollutants for the period
 877 1970–2012 within EDGAR v4. 3.2. *Earth Syst. Sci. Data*, 10(4), 1987-2013.
- 878 Da Silva, V. D. P. R., e Silva, R. A., Cavalcanti, E. P., Braga, C. C., de Azevedo, P. V.,
 879 Singh, V. P., & Pereira, E. R. R. (2010). Trends in solar radiation in NCEP/NCAR
 880 database and measurements in northeastern Brazil. *Solar Energy*, 84(10), 1852-
 881 1862.
- 882 de Jong, P., Barreto, T. B., Tanajura, C. A., Kouloukoui, D., Oliveira-Esquerre, K. P.,
 883 Kiperstok, A., & Torres, E. A. (2019). Estimating the impact of climate change on
 884 wind and solar energy in Brazil using a South American regional climate model.
 885 *Renewable energy*, 141, 390-401.
- 886 de Lima, F. J. L., Martins, F. R., Costa, R. S., Gonçalves, A. R., dos Santos, A. P. P., &
 887 Pereira, E. B. (2019). The seasonal variability and trends for the surface solar
 888 irradiation in northeastern region of Brazil. *Sustainable Energy Technologies and*
 889 *Assessments*, 35, 335-346.
- 890 Doelling, D. R., Loeb, N. G., Keyes, D. F., Nordeen, M. L., Morstad, D., Nguyen, C., ... &
 891 Sun, M. (2013). Geostationary enhanced temporal interpolation for CERES flux
 892 products. *Journal of Atmospheric and Oceanic Technology*, 30(6), 1072-1090.
- 893 Doelling, D. R., Sun, M., Nordeen, M. L., Haney, C. O., Keyes, D. F., & Mlynarczyk, P. E.
 894 (2016). Advances in geostationary-derived longwave fluxes for the CERES synoptic
 895 (SYN1deg) product. *Journal of Atmospheric and Oceanic Technology*, 33(3), 503-
 896 521.
- 897 Driemel, A., Augustine, J., Behrens, K., Colle, S., Cox, C., Cuevas-Agulló, E., ... & König-
 898 Langlo, G. (2018). Baseline Surface Radiation Network (BSRN): structure and data
 899 description (1992–2017). *Earth System Science Data*, 10(3), 1491-1501.

- 900 Dutton, E. G., Stone, R. S., Nelson, D. W., & Mendonca, B. G. (1991). Recent interannual
901 variations in solar radiation, cloudiness, and surface temperature at the South Pole.
902 *Journal of Climate*, 4(8), 848-858.
- 903 Feng, F., & Wang, K. (2019). Determining factors of monthly to decadal variability in
904 surface solar radiation in China: Evidences from current reanalyses. *Journal of*
905 *Geophysical Research: Atmospheres*, 124(16), 9161-9182.
- 906 Ferreira, G. W., & Reboita, M. S. (2022). A new look into the South America precipitation
907 regimes: Observation and Forecast. *Atmosphere*, 13(6), 873.
- 908 Fisch, G., MARENGO, J. A., & NOBRE, C. A. (1998). Uma revisão geral sobre o clima da
909 Amazônia. *Acta amazônica*, 28, 101-101.
- 910 Gilgen, H., Roesch, A., Wild, M., & Ohmura, A. (2009). Decadal changes in shortwave
911 irradiance at the surface in the period from 1960 to 2000 estimated from Global
912 Energy Balance Archive Data. *Journal of Geophysical research: atmospheres*,
913 114(D10).
- 914 Gueymard, C. A., & Yang, D. (2020). Worldwide validation of CAMS and MERRA-2
915 reanalysis aerosol optical depth products using 15 years of AERONET
916 observations. *Atmospheric Environment*, 225, 117216.
- 917 Hakuba, M. Z., Folini, D., & Wild, M. (2016). On the zonal near-constancy of fractional solar
918 absorption in the atmosphere. *Journal of Climate*, 29(9), 3423-3440.
- 919 Hersbach, H., Bell, B., Berrisford, P., Hirahara, S., Horányi, A., Muñoz-Sabater, J., ... &
920 Thépaut, J. N. (2020). The ERA5 global reanalysis. *Quarterly Journal of the Royal*
921 *Meteorological Society*, 146(730), 1999-2049.
- 922 IBGE. Censo Demográfico. Rio de Janeiro, Brazil: Fundação Instituto Brasileiro de
923 Geografia e Estatística. 2022. Available at:
924 <https://censo2022.ibge.gov.br/panorama/index.html> Last access: 01 Nov. 2023.
925 <https://censo2022.ibge.gov.br/panorama/index.html>
- 926 Inness, A., Ades, M., Agustí-Panareda, A., Barré, J., Benedictow, A., Blechschmidt, A. M., ...
927 & Suttie, M. (2019). The CAMS reanalysis of atmospheric composition.
928 *Atmospheric Chemistry and Physics*, 19(6), 3515-3556.
- 929 Jiao, B., Su, Y., Li, Q., Manara, V., & Wild, M. (2023). An integrated and homogenized
930 global surface solar radiation dataset and its reconstruction based on a convolutional
931 neural network approach. *Earth System Science Data*.
- 932 Kambezidis, H. D., Kaskaoutis, D. G., Kharol, S. K., Moorthy, K. K., Satheesh, S. K.,
933 Kalapureddy, M. C. R., ... & Wild, M. (2012). Multi-decadal variation of the net
934 downward shortwave radiation over south Asia: The solar dimming effect.
935 *Atmospheric Environment*, 50, 360-372.
- 936 Kazadzis, S., Founda, D., Psiloglou, B. E., Kambezidis, H., Mihalopoulos, N., Sanchez-
937 Lorenzo, A., ... & Nabat, P. (2018). Long-term series and trends in surface solar
938 radiation in Athens, Greece. *Atmospheric chemistry and physics*, 18(4), 2395-2411.
- 939 Kendall, M. G. (1975). Rank correlation methods. 2nd impression. *Charles Griffin and*
940 *Company Ltd. London and High Wycombe*.
- 941 Kudo, R., Uchiyama, A., Ijima, O., Ohkawara, N., & Ohta, S. (2012). Aerosol impact on the
942 brightening in Japan. *Journal of Geophysical Research: Atmospheres*, 117(D7).

- 943 Li, Z., Barker, H. W., & Moreau, L. (1995). The variable effect of clouds on atmospheric
944 absorption of solar radiation. *Nature*, *376*(6540), 486-490.
- 945 Liepert, B. G. (2002). Observed reductions of surface solar radiation at sites in the United
946 States and worldwide from 1961 to 1990. *Geophysical research letters*, *29*(10), 61-1.
- 947 Liley, J. B. (2009). New Zealand dimming and brightening. *Journal of Geophysical*
948 *Research: Atmospheres*, *114*(D10).
- 949 Lobo, C., & Cunha, J. M. P. D. (2019). Migração e mobilidade pendular nas áreas de
950 influência de metrópoles brasileiras. *Mercator (Fortaleza)*, *18*.
- 951 Long, C. N., & Dutton, E. G. (2002). BSRN Global Network Recommended QC Tests, V2.
952 0, BSRN Technical Report.
- 953 Long, C. N., Dutton, E. G., Augustine, J. A., Wiscombe, W., Wild, M., McFarlane, S. A., &
954 Flynn, C. J. (2009). Significant decadal brightening of downwelling shortwave in the
955 continental United States. *Journal of Geophysical Research: Atmospheres*,
956 *114*(D10).
- 957 Madhavan, B. L., Deneke, H., Witthuhn, J., & Macke, A. (2017). Multiresolution analysis of
958 the spatiotemporal variability in global radiation observed by a dense network of 99
959 pyranometers. *Atmospheric Chemistry and Physics*, *17*(5), 3317-3338.
- 960 Manara, V., Brunetti, M., Celozzi, A., Maugeri, M., Sanchez-Lorenzo, A., & Wild, M.
961 (2016). Detection of dimming/brightening in Italy from homogenized all-sky and
962 clear-sky surface solar radiation records and underlying causes (1959–2013).
963 *Atmospheric Chemistry and Physics*, *16*(17), 11145-11161.
- 964 Mann, H. B. (1945). Nonparametric tests against trend. *Econometrica: Journal of the*
965 *econometric society*, 245-259.
- 966 Natsis, A., Bais, A., & Meleti, C. (2023). Trends from 30-Year Observations of Downward
967 Solar Irradiance in Thessaloniki, Greece. *Applied Sciences*, *14*(1), 252.
- 968 Nishizawa, S., & Yoden, S. (2005). Distribution functions of a spurious trend in a finite
969 length data set with natural variability: Statistical considerations and a numerical
970 experiment with a global circulation model. *Journal of Geophysical Research:*
971 *Atmospheres*, *110*(D12).
- 972 Norris, J. R., & Wild, M. (2007). Trends in aerosol radiative effects over Europe inferred
973 from observed cloud cover, solar “dimming,” and solar “brightening”. *Journal of*
974 *Geophysical Research: Atmospheres*, *112*(D8).
- 975 Ohmura, A., & Lang, H. (1989). Secular variation of global radiation over Europe, in *Current*
976 *Problems in Atmospheric Radiation*. edited by J. Lenoble, & JF Geleyn, *98*, 301.
- 977 Ohmura, A., Dutton, E. G., Forgan, B., Fröhlich, C., Gilgen, H., Hegner, H., ... & Wild, M.
978 (1998). Baseline Surface Radiation Network (BSRN/WCRP): New precision
979 radiometry for climate research. *Bulletin of the American Meteorological Society*,
980 *79*(10), 2115-2136.
- 981 Ohmura, A. (2009). Observed decadal variations in surface solar radiation and their causes.
982 *Journal of Geophysical Research: Atmospheres*, *114*(D10).
- 983 Pfeifroth, U., Sanchez-Lorenzo, A., Manara, V., Trentmann, J., & Hollmann, R. (2018).
984 Trends and variability of surface solar radiation in Europe based on surface-and
985 satellite-based data records. *Journal of Geophysical Research: Atmospheres*,
986 *123*(3), 1735-1754.

- 987 Power, H. C. (2003). Trends in solar radiation over Germany and an assessment of the role of
988 aerosols and sunshine duration. *Theoretical and Applied Climatology*, 76(1), 47-63.
- 989 Raichijk, C. (2012). Observed trends in sunshine duration over South America. *International*
990 *Journal of Climatology*, 32(5), 669-680.
- 991 Reboita, M. S., Gan, M. A., Da Rocha, R. P., & Ambrizzi, T. (2010). Precipitation regimes in
992 South America: a bibliography review. *Revista Brasileira de Meteorologia*, 25(2),
993 185-204.
- 994 Rosário, N. E., Sauini, T., Pauliquevis, T., Barbosa, H. M., Yamasoe, M. A., & Barja, B.
995 (2019). Aerosol optical depth retrievals in central Amazonia from a multi-filter
996 rotating shadow-band radiometer calibrated on-site. *Atmospheric Measurement*
997 *Techniques*, 12(2), 921-934.
- 998 Russak, V. (1990). Trends of solar radiation, cloudiness and atmospheric transparency during
999 recent decades in Estonia. *Tellus B*, 42(2), 206-210.
- 1000 Schwartz, R. D. (2005). Global dimming: Clear-sky atmospheric transmission from
1001 astronomical extinction measurements. *Journal of Geophysical Research:*
1002 *Atmospheres*, 110(D14).
- 1003 Schwarz, M., Folini, D., Hakuba, M. Z., & Wild, M. (2018). From point to area: Worldwide
1004 assessment of the representativeness of monthly surface solar radiation records.
1005 *Journal of Geophysical Research: Atmospheres*, 123(24), 13-857.
- 1006 Schwarz, M., Folini, D., Yang, S., & Wild, M. (2019). The annual cycle of fractional
1007 atmospheric shortwave absorption in observations and models: spatial structure,
1008 magnitude, and timing. *Journal of Climate*, 32(20), 6729-6748.
- 1009 Schwarz, M., Folini, D., Yang, S., Allan, R. P., & Wild, M. (2020). Changes in atmospheric
1010 shortwave absorption as important driver of dimming and brightening. *Nature*
1011 *Geoscience*, 13(2), 110-115.
- 1012 Sen, P. K. (1968). Estimates of the regression coefficient based on Kendall's tau. *Journal of*
1013 *the American statistical association*, 63(324), 1379-1389.
- 1014 Silva Junior, C. H., Pessôa, A. C., Carvalho, N. S., Reis, J. B., Anderson, L. O., & Aragão, L.
1015 E. (2021). The Brazilian Amazon deforestation rate in 2020 is the greatest of the
1016 decade. *Nature ecology & evolution*, 5(2), 144-145.
- 1017 Stjern, C. W., Kristjánsson, J. E., & Hansen, A. W. (2009). Global dimming and global
1018 brightening—An analysis of surface radiation and cloud cover data in northern
1019 Europe. *International Journal of Climatology: A Journal of the Royal*
1020 *Meteorological Society*, 29(5), 643-653.
- 1021 Torres, O., Tanskanen, A., Veihelmann, B., Ahn, C., Braak, R., Bhartia, P. K., ... & Levelt, P.
1022 (2007). Aerosols and surface UV products from Ozone Monitoring Instrument
1023 observations: An overview. *Journal of Geophysical Research: Atmospheres*,
1024 112(D24).
- 1025 Vera, C., Baez, J., Douglas, M., Emmanuel, C. B., Marengo, J., Meitin, J., ... & Zipser, E.
1026 (2006). The South American low-level jet experiment. *Bulletin of the American*
1027 *Meteorological Society*, 87(1), 63-78.
- 1028 Wang, C., Jeong, G. R., & Mahowald, N. (2009). Particulate absorption of solar radiation:
1029 anthropogenic aerosols vs. dust. *Atmospheric Chemistry and Physics*, 9(12), 3935-
1030 3945.

- 1031 Wang, K., Ma, Q., Li, Z., & Wang, J. (2015). Decadal variability of surface incident solar
1032 radiation over China: Observations, satellite retrievals, and reanalyses. *Journal of*
1033 *Geophysical Research: Atmospheres*, 120(13), 6500-6514.
- 1034 Wang, X. L. (2008). Penalized maximal F test for detecting undocumented mean shift
1035 without trend change. *Journal of Atmospheric and Oceanic Technology*, 25(3), 368-
1036 384.
- 1037 Wild, M. (2009). Global dimming and brightening: A review. *Journal of Geophysical*
1038 *Research: Atmospheres*, 114(D10).
- 1039 Wild, M., Wacker, S., Yang, S., & Sanchez-Lorenzo, A. (2021). Evidence for clear-sky
1040 dimming and brightening in central Europe. *Geophysical Research Letters*, 48(6),
1041 e2020GL092216.
- 1042 Xia, X., Chen, H., Li, Z., Wang, P., & Wang, J. (2007). Significant reduction of surface solar
1043 irradiance induced by aerosols in a suburban region in northeastern China. *Journal of*
1044 *Geophysical Research: Atmospheres*, 112(D22).
- 1045 Yamasoe, M. A., Rosário, N. M. É., Almeida, S. N. S. M., & Wild, M. (2021). Fifty-six years
1046 of surface solar radiation and sunshine duration over São Paulo, Brazil: 1961–2016.
1047 *Atmospheric Chemistry and Physics*, 21(9), 6593-6603.
- 1048 Yang, S., Wang, X. L., & Wild, M. (2018). Homogenization and trend analysis of the 1958–
1049 2016 in situ surface solar radiation records in China. *Journal of Climate*, 31(11),
1050 4529-4541.
- 1051 Yuan, M., Leirvik, T., & Wild, M. (2021). Global trends in downward surface solar radiation
1052 from spatial interpolated ground observations during 1961–2019. *Journal of*
1053 *Climate*, 34(23), 9501-9521.
- 1054 Zuluaga, C. F., Avila-Diaz, A., Justino, F. B., & Wilson, A. B. (2021). Climatology and
1055 trends of downward shortwave radiation over Brazil. *Atmospheric Research*, 250,
1056 105347.

1057 Appendix

Station	Composite	Coordinates	Does it include SYNOP cloud cover?	% of monthly data available
Manaus	Manaus region	3.10S 60.01W	yes	87
Coari	Manaus region	4.10S 63.14W	yes	74
Rio Urubu	Manaus region	2.63S 59.60W	no	75
Urucará	Manaus region	2.53S 57.75W	no	82
Belém	Belém region	1.41S 48.43W	yes	95
Castanhal	Belém region	1.30S 47.94W	no	71
Tucuruí	Belém region	3.82S 49.67W	yes	92
Salinópolis	Belém region	0.62S 47.35W	no	69
Alta Floresta	South Amazon	10.07S 56.17W	no	62

Ariquemes	South Amazon	9.94S 62.96W	no	73
Juína	South Amazon	11.37S 58.77W	no	78
Porto Velho	South Amazon	8.79S 63.84W	no	73
Sorriso	South Amazon	12.55S 55.72W	no	85
Fortaleza	Fortaleza region	3.81S 38.53W	yes	68
Areia	Fortaleza region	6.97S 35.71W	yes	85
Caicó	Fortaleza region	6.46S 37.08W	yes	68
Natal	Fortaleza region	5.83S 35.20W	yes	65
Brasília	Midwest	15.78S 47.92W	yes	84
Goiânia	Midwest	16.64S 49.22W	yes	94
Campo Grande	Midwest	20.44S 54.72W	yes	79
Salvador	Salvador region	13.00S 38.50W	yes	89
Cruz das Almas	Salvador region	12.67S 39.08W	yes	66
Feira de Santana	Salvador region	12.19S 38.96W	yes	64
Itirucu	Salvador region	13.52S 40.11W	yes	61
Curitiba	South	25.44S 49.23W	yes	72
Porto Alegre	South	30.05S 51.17W	yes	95
Santa Maria	South	29.72S 53.72W	yes	89
Florianópolis*	South	27.60S 48.52W	yes	
Campos do Jordão	Southeast	22.75S 45.60W	yes	69
Monte Verde	Southeast	22.86S 46.04W	no	84
Rio de Janeiro - Marambaia	Southeast	23.05S 43.59W	yes	78
Seropédica	Southeast	22.75S 43.68W	no	98
São Paulo*	Southeast	23.65S 46.62W	yes	99

1058

1059

1060

1061

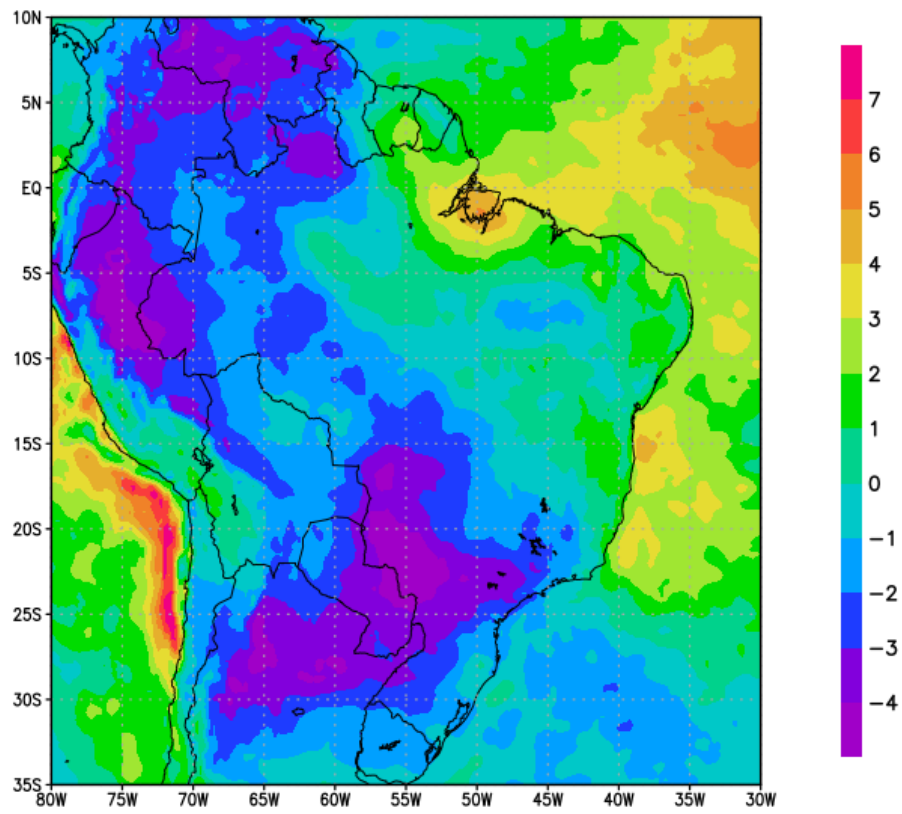
1062

1063

1064

Table 3: Stations used in the study, the composites they were associated with, their coordinates, information whether Synop cloud cover data was available and the percentage of months with available data (out of all the months in the period used for the respective composite - see table 1). *Stations not from the Brazilian National Institute of Meteorology. Florianópolis station from BSRN; São Paulo station from the Institute for Astronomy, Geophysics and Atmospheric Sciences at the University of São Paulo.

1065



1066

1067 **Figure A1 - Total cloud cover trends for the 1990-2006 period (in % per decade) from ERA5.**